Title

Formation of an ultracarbonaceous Antarctic micrometeorite through minimal aqueous alteration in a small porous icy body

Authors

Yabuta, Hikaru

Noguchi, Takaaki

Itoh, Shoichi

et al.

Publication Date

2017-10-01

DOI

10.1016/j.gca.2017.06.047

Available online at www.sciencedirect.com

ScienceDirect

Geochimica et Cosmochimica Acta 214 (2017) 172–190

Geochimica et Cosmochimica Acta

www.elsevier.com/locate/gca

Formation of an ultracarbonaceous Antarctic micrometeorite through minimal aqueous alteration in a small porous icy body

Hikaru Yabuta [a,*], Takaaki Noguchi [b], Shoichi Itoh [c], Tomoki Nakamura [d], Akira Miyake [c], Shinichi Tsujimoto [e], Noriaki Ohashi [e], Naoya Sakamoto [f], Minako Hashiguchi [g], Ken-ichi Abe [f], Aya Okubo [h], A.L. David Kilcoyne [i], Shogo Tachibana [f], Ryuji Okazaki [g], Kentaro Terada [j], Mitsuru Ebihara [k], Hiroko Nagahara [h]

[a] *Department of Earth and Planetary Systems Science, Hiroshima University, 1-3-1 Kagamiyama, Hiroshima 739-8526, Japan*
[b] *Faculty of Arts and Science, Kyushu University, 744 Motooka, Nishi-ku, Fukuoka 819-0395, Japan*
[c] *Faculty of Science, Kyoto University, Kitashirakawa Oiwake-cho, Sakyo-ku, Kyoto 606-8502, Japan*
[d] *Department of Earth Science, Tohoku University, 6-3 Aramaki Aza Aoba, Aoba, Sendai, Miyagi 980-8578, Japan*
[e] *College of Science, Ibaraki University, 2-1-1, Bunkyo, Mito 310-8512, Japan*
[f] *Department of Natural History Sciences, Hokkaido University, N10W8, Kita-ku, Sapporo 060-0810, Japan*
[g] *Faculty of Science, Kyushu University, 744 Motooka, Nishi-ku, Fukuoka 819-0395, Japan*
[h] *Department of Earth and Planetary Science, The University of Tokyo, 7-3-1 Hongo, Bunkyo-ku, Tokyo 113-0033, Japan*
[i] *Advanced Light Source, Lawrence Berkeley National Laboratory, 6 Cyclotron Rd., Berkeley, CA, USA*
[j] *Department of Earth and Space Science, Osaka University, 1-1 Machikaneyama, Toyonaka, Osaka 560-0043, Japan*
[k] *Department of Chemistry, Tokyo Metropolitan University, 1-1 Minami-Osawa, Hachioji, Tokyo 192-0397, Japan*

Received 30 May 2016; accepted in revised form 29 June 2017; available online 12 July 2017

Abstract

A comprehensive study of the organic chemistry and mineralogy of an ultracarbonaceous micrometeorite (UCAMM D05IB80) collected from near the Dome Fuji Station, Antarctica, was carried out to understand the genetic relationship among organic materials, silicates, and water. The micrometeorite is composed of a dense aggregate of ~5 μm-sized hollow ellipsoidal organic material containing submicrometer-sized phases such as glass with embedded metal and sulfides (GEMS) and mineral grains. There is a wide area of organic material (~15 × 15 μm) in its interior. Low-Ca pyroxene is much more abundant than olivine and shows various Mg/(Mg + Fe) ratios ranging from ~1.0 to 0.78, which is common to previous works on UCAMMs. By contrast, GEMS grains in this UCAMM have unusual chemical compositions. They are depleted in both Mg and S, which suggests that these elements were leached out from the GEMS grains during very weak aqueous alteration, without the formation of phyllosilicates.

The organic materials have two textures—smooth and globular with an irregular outline—and these are composed of imine, nitrile and/or aromatic nitrogen heterocycles, and amide. The ratio of nitrogen to carbon (N/C) in the smooth region of the organics is ~0.15, which is five times higher than that of insoluble organic macromolecules in types 1 and 2 carbonaceous chondritic meteorites. In addition, the UCAMM organic materials are soluble in epoxy and are thus hydrophilic; this polar nature indicates that they are very primitive. The surface of the material is coated with an inorganic layer, a few

* Corresponding author. Fax: +81 82 424 0735.
E-mail address: hyabuta@hiroshima-u.ac.jp (H. Yabuta).

http://dx.doi.org/10.1016/j.gca.2017.06.047

nanometers thick, that consists of C, O, Si, S, and Fe. Sulfur is also contained in the interior, implying the presence of organosulfur moieties. There are no isotopic anomalies of D, ^{13}C, or ^{15}N in the organic material.

Interstellar photochemistry alone would not be sufficient to explain the N/C ratio of the UCAMM organics; therefore, we suggest that a very small amount of fluid on a comet must have been necessary for the formation of the UCAMM. The GEMS grains depleted in Mg and S in the UCAMM prove a very weak degree of aqueous alteration; weaker than that of carbonaceous chondrites. Short-duration weak alteration probably caused by planetesimal shock locally melted cometary ice grains and released water that dissolved the organics; the fluid would likely have not mobilized because of the very low thermal conductivity of the porous icy body. This event allowed the formation of the large organic puddle of the UCAMM, as well as organic matter sulfurization, formation of thin membrane-like layers of minerals, and deformation of organic nanoglobules.

Keywords: Ultracarbonaceous Antarctic micrometeorites; Organic matter; GEMS; Aqueous alteration; Comet; Shock; SIMS; XANES; TEM

1. INTRODUCTION

The interstellar dusts that accrete to form a protoplanetary disk are thought to be micron-sized particles consisting of an amorphous silicate core, a refractory organic mantle, and an outer mantle of ice (Greenberg and Li, 1997). As there is a large difference in the thermal stability of these three components, the composition of the grains is expected to change as a result of thermal processing in the protoplanetary disk. The association of reactive components, amorphous silicates, organic materials, and water in a single grain suggests possible interactions among the three components. It has been well recognized recently that organic materials in chondrites are the aqueously and/or thermally processed products from parent bodies and that their chemical and isotopic signatures have been modified (e.g., Alexander et al., 2007). However, the identity of the precursor materials and the conditions under which the organics were processed in the chondrite parent bodies are not known. Therefore, it is important to trace back the evolution and interactions among silicates, organic materials, and ice in the proto-solar disk and their consequence in the parent bodies. This task requires us to study organics that are as primitive as possible, which might correspond to materials other than those found in chondrites.

Interplanetary dust particles (IDPs) and Antarctic micrometeorites (AMMs) are among the most primitive solar system materials available to us and are among the most suitable objects for an *in-situ* study on the origins of and the spatial relationships between organic and inorganic materials formed in the early solar system. Chondritic porous (CP)-IDPs are thought to have a link with short period comets (Messenger et al., 2006), based on their fine-grained, porous, and fragile structure (Bradley and Brownlee, 1986), high abundance of carbon (~12%; Thomas et al., 1994), and the presence of sub-micron silicate glass with embedded metal and sulfides (GEMS) (Bradley et al., 1999). It also has been known that D- and ^{15}N-enrichments of the organics in CP-IDPs (e.g. Messenger, 2000; Floss et al., 2004) and IDPs from the comet 26P/Grigg–Skjellerup dust stream (Busemann et al., 2009) resemble those found in primitive types 1 and 2 carbonaceous chondrites (Busemann et al., 2006; Nakamura-Messenger et al., 2006). Recently, AMMs containing porous aggregates of GEMS and enstatite whiskers/platelets, which have similar morphology and mineralogy to CP-IDPs, have been identified (Noguchi et al., 2015). Both IDPs and AMMs are thus key extraterrestrial materials that can be used to enhance our understanding of the relationship between comets and meteorites.

Of the AMMs, ultracarbonaceous micrometeorites (UCAMMs) are unique extraterrestrial materials that contain a large amount of carbonaceous materials. They were collected for the first time by the 46th and 47th Japan Antarctic Research Expedition (JARE) teams from the virgin surface snow near the Dome Fuji Station, Antarctica, and were reported to be pristine in terms of mineralogy and chemistry (Nakamura et al., 2005). One of the UCAMMs contains light noble gases with a solar wind origin, and two contain an abundance of presolar grains (Yada et al., 2008; Floss et al., 2012). UCAMMs have been found independently in Antarctica by a French-Italian team, and these are characterized by D-enrichment in organic matter (Duprat et al., 2010). The D-enrichment is 10–30 times the terrestrial value. Duprat et al. (2010) noted that the organic materials in UCAMMs could be produced in the outer protoplanetary disk, based on the identification of crystalline minerals that are thought to be of solar origin and are embedded in the organic material. Dartois et al. (2013) reported ^{15}N- and D-rich micrometeorites, and proposed that the nitrogen-rich organic material in UCAMMs was formed in the Oort cloud by irradiation of ice rich in CH_4 and N_2.

In this paper, we describe our comprehensive mineralogical and organic chemical study of an UCAMM and suggest a new pathway for the formation of UCAMMs through the interaction of organics, silicates, and water in the very early stage of alteration in a parent body.

2. EXPERIMENTAL

Antarctic snow collected by the 51st JARE team of the National Institute of Polar Research (NIPR) was melted and filtered in a class 1000 clean room at Ibaraki University, and the residual particles were manually picked under a binocular microscope. Details of the micrometeorite collection method are described by Sakamoto et al. (2010). The particles were observed with a JEOL JSM-5600LV scanning electron microscope (SEM) equipped with an energy disper-

sive spectrometer (EDS) at Ibaraki University, and micrometeorites were selected from terrestrial materials based on their morphology and EDS spectra with chondritic composition rich in Si, Mg, Fe, and O (electronic supplementary data, S1). About 90 micrometeorites were identified from fine-grained particles collected from ~100 kg of snow. When the intensity of the C kα peak exceeded twice that of the O kα, the particle was classified as an UCAMM; only one, D05IB80, was so identified. The bulk mineralogy of D05IB80 was investigated by using synchrotron radiation X-ray diffraction (SR-XRD) at the Photon Factory Institute of Materials Structure Science, High Energy Accelerator Research Organization, Tsukuba, Japan. Detailed procedures were given in Nakamura et al. (2011).

Raman spectroscopy of the UCAMM D05IB80 was performed using a JASCO NRS-3100 Raman spectrometer equipped with a 785 nm excitation laser at Ibaraki University. The beam diameter of the laser was ~2 μm, and the laser power was suppressed to below 1 mW to avoid decomposition of the carbonaceous material.

Next, UCAMM D05IB80 was embedded in epoxy resin and ultramicrotomed into sections 70 nm thick. After ultramicrotomy, the potted butt of the micrometeorite was embedded again in epoxy resin and the surface was polished to make a flat epoxy disk (6 mm in diameter) for isotopic mapping analysis with a secondary ion mass spectroscopy (SIMS) at Hokkaido University (Cameca ims-1270 SIMS equipped with SCAPS) (Yurimoto et al., 2003). Schematic diagrams showing the 3D relationships among the ultrathin samples (ultramicrotomed sections and an FIB section) and the flat sample of this UCAMM are presented in the electronic supplementary data S2.

An ~100 to ~200 pA Cs^+ primary beam in the aperture illumination mode of the SIMS was used to achieve uniform secondary ion emission from a sample area of ~30 × 40 μm^2. A normal-incident electron gun was used to compensate for sample charging, and the exit slit was narrow enough to eliminate the contribution of interference ions to the isotope images. Isotopographs of $^{16}O^-$, $^{12}C^{14}N^-$, $^{32}S^-$, $^1H^-$, $^2D^-$, $^1H^-$, $^{16}O^-$, $^{12}C^{14}N^-$, and $^{32}S^-$ were acquired in this order, where a 150 μm contrast aperture (CA) was applied for H and D isotopographs and a 50 μm CA was used for $^{16}O^-$, $^{12}C^{14}N^-$, and $^{32}S^-$ isotopographs in order to obtain high lateral spatial resolution. The exposure time was 20 s for H^-, 1000 s for D^-, 20 s for $^{16}O^-$, 20 s for $^{12}C^{14}N^-$, and 40 s for $^{32}S^-$, respectively. We obtained secondary ion images of $^{12}C^{14}N^-$, $^{12}C^{15}N^-$, $^{12}C^{14}N^-$, $^{12}C^-$, $^{13}C^-$, and $^{12}C^-$ sequentially for the second session after FIB. A 50 μm CA was used for $^{12}C^{14}N^-$, $^{12}C^{15}N^-$, $^{12}C^-$, and $^{13}C^-$ isotopographs. The exposure time was 50 s for $^{12}C^{14}N^-$, 400 s for $^{12}C^{15}N^-$, 50 s for $^{12}C^-$, and 500 s for $^{13}C^-$.

The H, N, and C isotopic compositions were represented by δ-value notation:

$$\delta D_{SMOW} = \left\{ \frac{(D/H)_{sample}}{(D/H)_{SMOW}} - 1 \right\} \times 1000$$

$$\delta^{15}N_{AIR} = \left\{ \frac{(^{15}N/^{14}N)_{sample}}{(^{15}N/^{14}N)_{AIR}} - 1 \right\} \times 1000$$

$$\delta^{15}C_{PDB} = \left\{ \frac{(^{15}C/^{12}C)_{sample}}{(^{13}C/^{12}C)_{PDB}} - 1 \right\} \times 1000$$

where SMOW denotes Standard Mean Ocean Water, AIR denotes the Earth's atmosphere, and PDB denotes Pee Dee Belemnite. The instrumental mass fractionations for the D/H, $^{15}N/^{14}N$, and $^{13}C/^{12}C$ ratios of the epoxy were corrected by assuming that the δD, $\delta^{15}N$, and $\delta^{13}C$ values are 0‰, respectively, and that the matrix effects are the same for the epoxy and the organic matters in the UCAMM. Therefore, the δ-values of the organic matter shown here are the values relative to the epoxy. The isotope ratio image was obtained by averaging 5 × 5 pixels (corresponding to 1.0 × 1.0 μm^2) for δD and 3 × 3 pixels (corresponding to 0.6 × 0.6 μm^2) for $\delta^{15}N$ and $\delta^{13}C$ in order to reduce the statistical error. The lateral resolutions of the isotopographs are ~1 μm for $^1H^-$ and $^2D^-$ and ~0.6 μm for $^{12}C^-$, $^{13}C^-$, $^{12}C^{14}N^-$, $^{12}C^{15}N^-$, $^{32}S^-$, and $^{16}O^-$.

The morphology of the UCAMM was observed by an FE-SEM-EDS (JSM-7000F, Oxford INCA Energy) system at Hokkaido University after the isotope microscopy analyses, and a 200 nm thick section was prepared by the dual beam focused ion beam and scanning electron microscope (FIB-SEM) JEOL JIB-4501 at Ibaraki University for further analyses.

C-, N-, and O- X-ray absorption near edge structure (XANES) spectra of the FIB section were acquired by using scanning transmission X-ray microscopy (STXM) at the beamline (BL) 5.3.2.2 of the Advanced Light Source (ALS) at the Lawrence Berkeley National Laboratory (Kilcoyne et al., 2003). The beamline employs a bending magnet providing a useful photon range spanning ~250 to 800 eV with a flux of 10^7 photons per second. Energy selection on BL5.3.2 is performed with a low-dispersion spherical grating monochromator and affords an energy resolution (E/ΔE) of 5000. Carbon-XANES transmission spectra were obtained in the stack scan mode with 0.1-eV resolution across the near edge region and 0.5-eV resolution below and above the near edge absorption. Energy calibration was conducted by measuring CO_2 and N_2 gas prior to the measurements. The absorption spectra (optical density, OD) were obtained as $OD = -\ln(I/I_0)$, where I is the X-ray intensity transmitted from sample and I_0 is that recorded without sample. Leinweber et al. (2007) and Cody et al. (2008) were referred to for the absorption peak assignment.

The FIB section was observed under a polarizing microscope to check the textural relationships between the MM and the epoxy resin in the section. The section was further observed with a JEOL JEM-2100F field emission TEM equipped with a JEOL JED SDD EDS for detailed textural observation and elemental analysis at the JEOL Corporation and with a JEOL JEM-2100 equipped with an Oxford INCA SDD EDS at Ibaraki University.

3. RESULTS

3.1. Texture and mineralogy

Fig. 1a shows a secondary electron image of an UCAMM D05IB80, which is about ~40 × 30 μm in size.

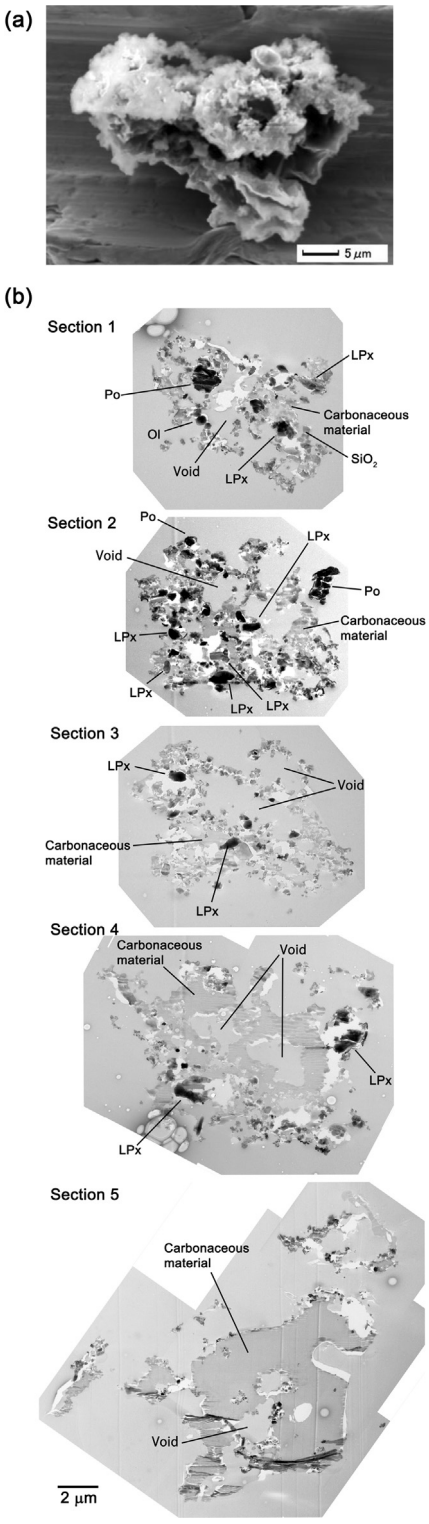

Fig. 1. (a) Secondary electron image of the ultracarbonaceous micrometeorite (UCAMM) D05IB80 placed on a platinum plate. The upper half of the UCAMM is porous and covered by fine-grained (typically submicrometer) particles, whereas the lower half is smooth. (b) Bright-field (BF) TEM images of ultramicrotomed sections of the UCAMM D05IB80. Each section was selected out of every three to five serial sections. Abbreviations: LPx, low-Ca pyroxene; PO, pyrrhotite; Ol, Olivine.

There are abundant submicrometer-size constituents on the surface of the upper half of this UCAMM. By contrast, the other half is poor in submicrometer constituents and has a smooth surface. Ultramicrotomed sections of the UCAMM are shown in Fig. 1b. The sections were selected out of every 3–5 serial sections. There are many mineral grains in sections No. 1 and 2 (Fig. 1b), which may correspond to the sections of the upper half of the UCAMM shown in Fig. 1a. There are voids in each section, which are composed of densely packed hollow organic material with ~0.5 to ~2 μm thick walls containing minerals.

TEM observation shows that this UCAMM contains GEMS (Fig. 2a and b), which is common to chondritic porous (CP) IDPs (e.g. Bradley and Dai, 2004), UCAMMs previously investigated (Nakamura et al., 2005; Duprat et al., 2010; Dobrică et al., 2012), and CP MMs (Noguchi et al., 2015). Their typical size ranges from ~200 to ~400 nm in diameter, and they contain tiny grains (<30 nm) of Fe sulfide as well as rare Fe metal, which appear as S- and Fe-enriched spots in the elemental distribution maps (Fig. 2c). O, Al, and Si are homogeneously distributed and Mg is heterogeneously distributed in the glassy (amorphous silicate) matrix of this GEMS grain (Fig. 2c).

Olivine, low-Ca pyroxene, high-Ca pyroxene, amorphous silica, and pyrrhotite are major inorganic phases in this UCAMM (Fig. 2d–i), and low-Ca pyroxene and pyrrhotite are more abundant than the other phases. Among these phases, amorphous silica containing no other elements is rare in CP IDPs (e.g. Bradley and Dai, 2004), CP MMs (e.g. Noguchi et al., 2015), and UCAMMs investigated previously (Dobrică et al., 2012). No hydrated silicate was found in the UCAMM.

The major element compositions of the olivine, pyroxene, and pyrrhotite in the UCAMM D05IB80 are shown in Fig. 3 and Table 1. The majority of the GEMS grains in this UCAMM are highly depleted in Mg relative to [Si + Al] and Fe and plot at the Mg-poor end of the GEMS grains in CP IDPs (Fig. 3a). In addition, sulfur is also depleted in the GEMS grains (Fig. 3b). These data strongly suggest that the GEMS grains in this MM do not retain their original chemical compositions.

Olivine is a minor phase in this MM, and the forsterite mol% ranges from ~100 to 89 (Fig. 3c). The low-Ca pyroxene shows a variation of enstatite mol% from ~100 to 78 (Fig. 3c). Because all of the high-Ca pyroxene grains analyzed contain high Al_2O_3 contents ranging from 14.7 to 27.8 wt%, they plot around the Di apex or outside the pyroxene quadrilateral due to the relative deficiency of Mg^{2+} and Fe^{2+} caused by substitution of Al^{3+} in high-Ca pyroxene (Fig. 3c). FeO vs MnO and FeO vs Cr_2O_3 wt% diagrams show that some low-Ca pyroxene crystals have high MnO (up to 1.85 wt%) and high Cr_2O_3 (up to 2.32 wt%) contents relative to FeO contents (Fig. 3e and f). Most pyrrhotite crystals are poor in Ni. Only two crystals have 2.8 and 3.2 Ni atomic%, respectively (Fig. 3d). These data are consistent with the chemical compositions of olivine, pyroxene, and pyrrhotite in CP IDPs, previously reported UCAMMs, and mineral grains recovered from 81P/Wild 2 (Klöck and Stadermann, 1994; Zolensky and Barrett, 1994; Zolensky et al., 2006;

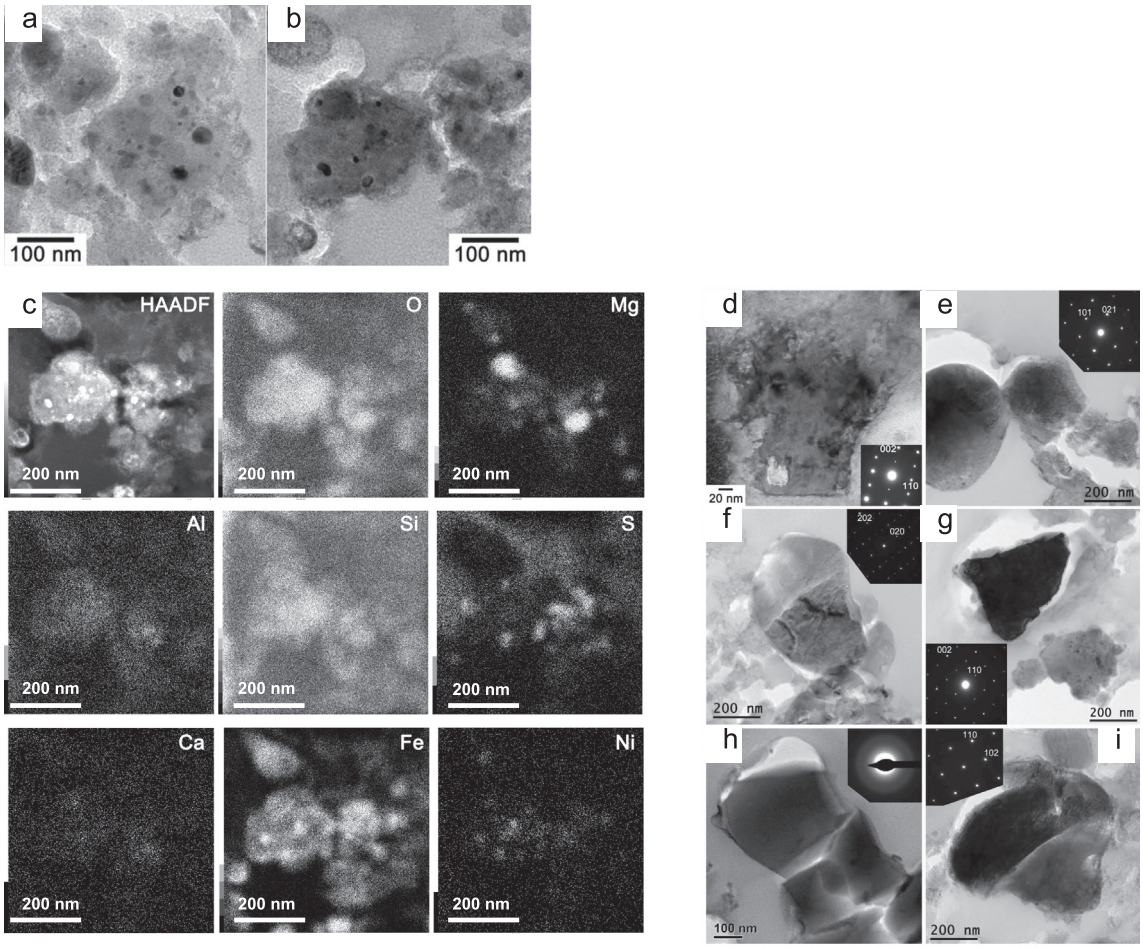

Fig. 2. (a, b) BF-TEM images of GEMS grains in the UCAMM D05IB80. (c) HAADF-STEM image and elemental distribution maps of the same GEMS grains in (b). (d–i) BF TEM images of minerals in an FIB section and ultrathin sections of D05IB80: (d) olivine crystal in the FIB sections, (e–i) olivine, low-Ca pyroxene, high-Ca pyroxene, amorphous silica, and pyrrhotite in ultrathin sections. The inset in each TEM image is a selected area electron diffraction (SAED) pattern of each phase.

Joswiak et al., 2009, 2012; Dobrică et al., 2012; Frank et al., 2014).

3.2. Organic material: size, texture, molecular and isotopic compositions

3.2.1. Size

Fig. 4 shows the isotopographs of $^{12}C^{14}N^-$, $^{32}S^-$, and $^{16}O^-$ along with the backscattered electron (BSE) image of the UCAMM D05IB80. The distribution of $^{12}C^{14}N^-$ indicates that the size of organic carbon is ~15 μm × 15 μm. Compared to the typical size of organic carbon in chondritic meteorites (a few hundreds of nm) (e.g. Le Guillou et al., 2014) and that of comet Wild 2 dust particles (~1–2 μm) (Cody et al., 2008), the organics in the present study are extraordinarily large. $^{32}S^-$ and $^{16}O^-$ are concentrated in the rim of the organic material (Fig. 4), and $^{32}S^-$ is also distributed within the organic material, although its abundance is lower than in the rim.

3.2.2. Observation of soluble organics

UCAMM D05IB80 was originally almost opaque under a transmitted light, although a translucent brown-colour part seeped from the sample when it was embedded in epoxy (Fig. 5b). A certain degree of affinity between the UCAMM and the epoxy seems to have taken place, which is shown by the observation that the boundary between the embedding epoxy (light brown) and the UCAMM (dark brown) is less clear in the transmitted optical image (Fig. 5d) than in the high-angle annular dark-field scanning transmission electron microscopy (HAADF-STEM) image (Fig. 5e).

3.2.3. Molecular compositions

A Raman spectrum of carbonaceous material in UCAMM D05IB80 is shown in Fig. 6. The spectrum is broad, and the centers and full width at half maximum (FWHM) of D_1 and G are 1338 cm^{-1} (ω_{D1}) and 369 cm^{-1} (Γ_{D1}) and 1569 cm^{-1} (ω_G) and 109 cm^{-1} (Γ_G), respectively. Although the analytical conditions were different from

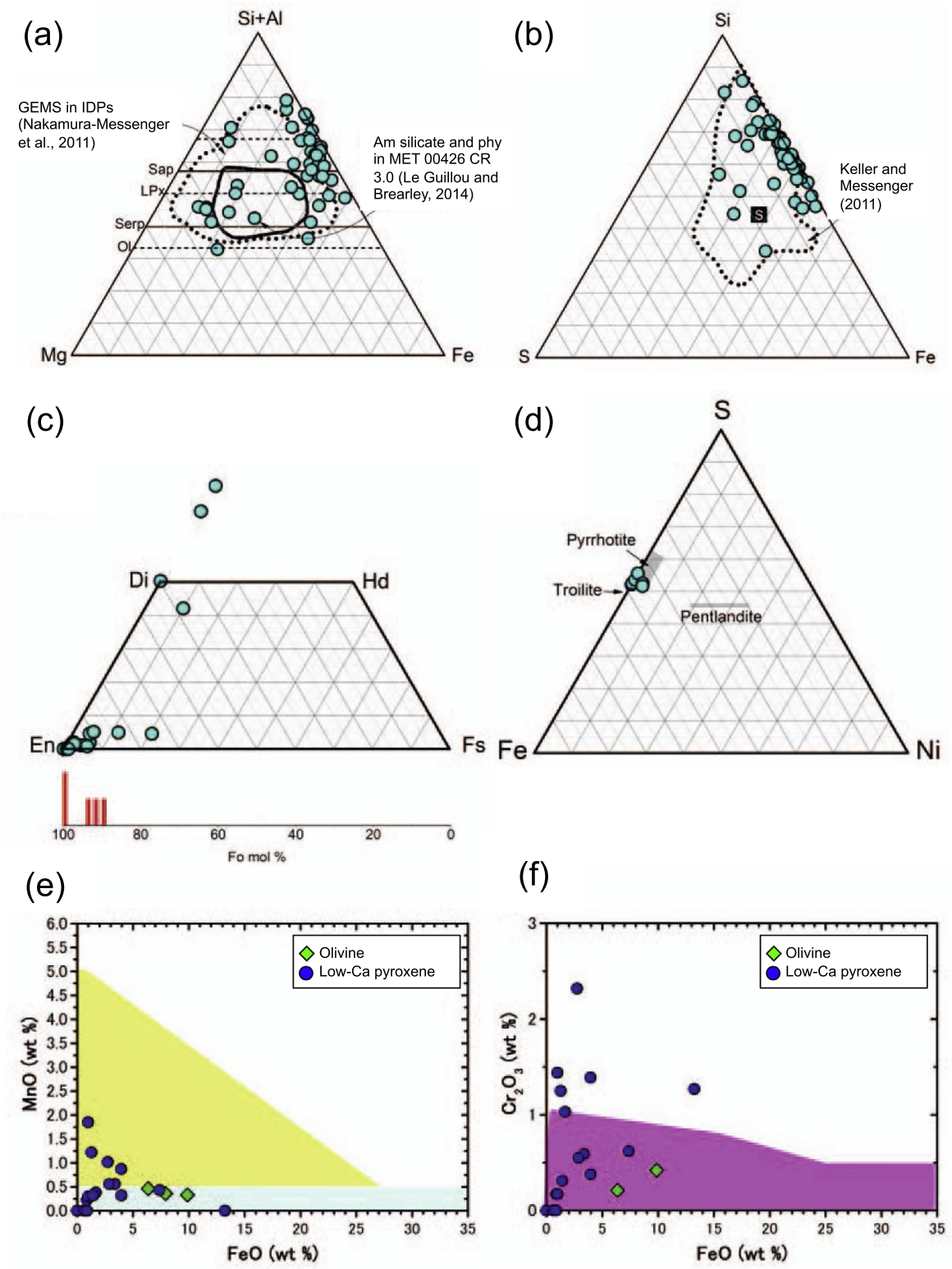

Fig. 3. Chemical compositions of phases in the UCAMM D05IB80. (a) [Si + Al]–Mg–Fe ternary diagram and (b) Si–S–Fe ternary diagram of GEMS grains. (c) Pyroxene quadrilateral showing the chemical compositions of low- and high-Ca pyroxenes and a forsterite (Fo) mol.% histogram of olivine. (d) S–Fe–Ni ternary diagram of pyrrhotite. (e) FeO vs MnO and (f) FeO vs Cr_2O_3 diagrams of olivine and low-Ca pyroxene.

Table 1
Representative chemical compositions of phases in UCAMM D05IB80. 100 wt% normalized.

Mineral	Ol	LPx	HPx	Silica	GEMS	GEMS		Po
SiO_2	41.88	57.68	47.38	100	57.37	45.26	S	39.86
TiO_2	b. d.	b. d.	1.52	b. d.	b. d.	b. d.	Fe	59.9
Al_2O_3	b. d.	b. d.	14.98	b. d.	4.05	3.22	Ni	0.23
Cr_2O_3	0.21	0.55	b. d.	b. d.	0.52	0.58	Total	100
FeO	6.37	2.88	b. d.	b. d.	31.39	17.02		
NiO	b. d.	b. d.	b. d.	b. d.	b. d.	0.62		
MnO	0.46	0.56	b. d.	b. d.	b. d.	b. d.		
MgO	51.08	37.74	15	b. d.	3.28	29.45		
CaO	b. d.	0.59	21.12	b. d.	1.12	0.52		
Na_2O	b. d.	b. d.	b. d.	b. d.	b. d.	1.74		
K_2O	b. d.	b. d.	b. d.	b. d.	1.1	b. d.		
SO_3	b. d.	b. d.	b. d.	b. d.	1.08	3.32		
Total	100	100	100	100	100	100		
Fo mol%	93.5							
Wo mol%		1.06	50.32[a]					
En mol%		94.88	49.68[a]					
Fs mol%		4.06	0.0[a]					

Abbreviations: Ol, olivine; LPx, low-Ca pyroxene; HPx, high-Ca pyroxene; GEMS, glass with embedded metal and sulfide; Po, pyrrhotite.
[a] These values were calculated after subtraction of Calcium tschermakite component $CaAl_2SiO_6$.

those of the other studies that investigated CP IDPs, MMs, and carbonaceous chondrites (e.g. Rotundi et al., 2008; Busemann et al., 2009; Dobrică et al., 2011; Dartois et al., 2013), the peak broadness and the wave parameters indicate that the carbonaceous material is very disordered.

By combining C- and N-XANES maps of the FIB section, we can distinguish the organic nitrogen-rich regions of the UCAMM from the epoxy that does not contain N (Fig. 7a and b). Nitrogen-XANES spectra of N-rich regions 1 and 2 (Fig. 7d) exhibit intense peaks of 1s-π^* transitions of imine (C═N*) at 398.8 eV (peak E), aromatic nitrogen heterocycles (C—N*═C) and/or nitrile (C≡N*) at 399.7 eV (peak F), and amide (N*Hx(C═O)C) at ~401.5 eV (peak G). The N-XANES spectra provided a sufficient signal- to-noise (S/N) ratio, which has not generally been observed in chondritic insoluble organic matter and even in organic matter in IDPs (Cody et al., 2011). The relative peak intensity of nitrogen heterocycles in region 2 is higher than that in region 1. The nitrogen speciation improves the characterization of carbon functional groups in C-XANES spectra (Fig. 7c). The peak A at ~285 eV is assigned to 1s-π^* transitions of aromatic/unsaturated carbon (C═C*), which probably includes aromatic nitrogen heterocycles (e.g. pyridine) in regions 1 and 2, due to the presence of imine in their N-XANES. The peak B at ~286.6 eV is derived from 1s-π^* transitions of nitrile/aromatic N or vinyl-keto carbon. The presence of nitrile/aromatic N is very likely because of the intense peaks (peak G) in the N-XANES of regions 1 and 2, whereas the same peak in the epoxy region would be assigned to the vinyl-keto group due to the absence of N. A broad peak ranging from 287 to 288 eV for regions 1 and 2 includes a peak of 1s-3p/σ^* transition to aliphatic carbon (peak C) and a peak D at ~288.3 eV assigned to 1s-π^* transitions of carboxyl carbon (C*═O) and/or amidyl carbon (NHx(C*═O)C). The N/C ratio for region 1 was calculated from the spectral fitting using aXis 2000 software to be 0.15 ± 0.03, and the O/C ratio is 0.27 ± 0.02. There is a possibility that the XANES results in the present work may be affected by FIB-induced damage, such as an increase of the aromatic carbon (De Gregorio et al., 2010; Bassim et al., 2012). In that case, the original peak intensity of imine may have been relatively lower and those of nitrile and carboxyl groups may have been higher than the acquired spectra. Nevertheless, the possible modification of functional group compositions by FIB should not affect the elemental ratios. Sulfur-XANES measurement was carried out at the BL 5.3.2.1 with a photon energy range of 600–2000 eV, ALS, but the sulfur abundance in the FIB section was below the detection limit of XANES.

3.2.4. Texture

TEM observation of the organic N-rich material indicates the presence of two N-rich regions: region 1 is smooth and region 2 is entirely globular (Fig. 8). The two regions are connected at the bottom-left corner of the FIB section (Fig. 5e), indicating that these regions were made of the same organic material as shown in the similar C- and N-XANES spectra (Fig. 7c and d). The globules in region 2 appear similar in size (a few hundred nm) to the organic nanoglobules ubiquitously observed in chondritic meteorites (e.g. Nakamura et al., 2002; Garvie and Buseck, 2004; Nakamura-Messenger et al., 2006; Peeters et al., 2012; De Gregorio et al., 2013; Matsumoto et al., 2013), micrometeorites (Sakamoto et al., 2010), IDPs (Busemann et al., 2009), and comet Wild 2 dust particles (De Gregorio et al., 2010, 2011). However, the organic nanoglobules in UCAMM D05IB80, forming aggregates, have more irregular shapes compared to the rounded globules in most carbonaceous chondrites. The nanoglobules appear to contain fillings in their interiors (Fig. 8b and c). A high-resolution TEM image of the globule filling, which

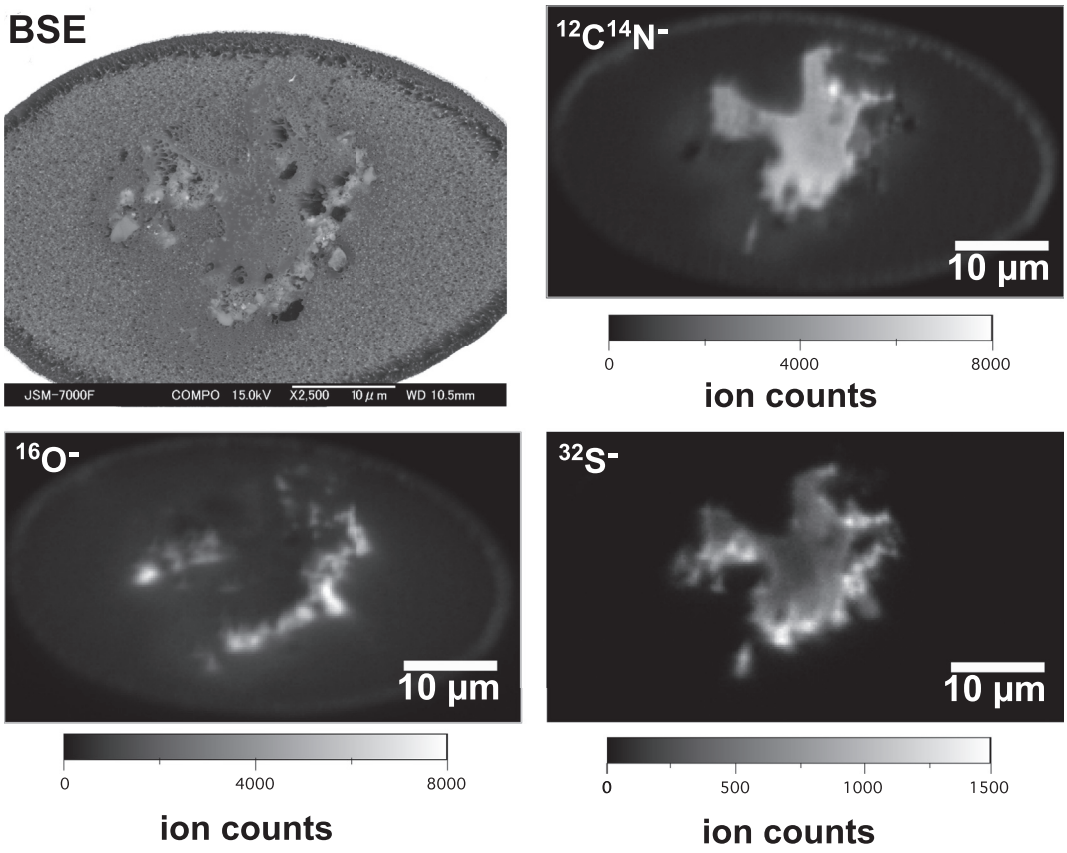

Fig. 4. BSE image after SIMS analysis and $^{12}C^{14}N^-$, $^{16}O^-$ and $^{32}S^-$ isotopographs of UCAMM D05IB80.

is an aggregate of tiny crystals, is shown in Fig. 9(c). Although the EDS spectrum of the aggregate suggests that it is composed of low-Ca pyroxene, it was impossible to determine the phase of the crystals due to their small sizes.

TEM images (Fig. 8b and c) revealed that the globular region has three very thin (<5 nm) surface layers, that the smooth region has two (Fig. 8d and e), and that the surface layer is less electron-transparent than the interior. The less electron-transparent material is estimated to be amorphous due to the absence of lattice fringes, and it is rich in C, O, Si, S, and Fe (Fig. 9), suggesting the presence of silicate and sulfide. The high-resolution TEM image of the thin layers in the globular region revealed that the layers contain nanocrystals. Although 0.24- and 0.28-nm lattice fringes were observed (Fig. 8f), we could not obtain diffraction spots in the selected area electron diffraction (SAED) patterns, which gave only halo patterns. This is probably due to the minute volumes of these nanocrystals. Therefore, we could not identify the phase of these nanocrystals. By contrast, we could not find any nanocrystals at the smooth boundaries (Fig. 8g). The thin layers are thought to be indigenous and are neither reaction products with epoxy resin nor reaction products with filtrated water in the Antarctica snow, because the layers are specifically present only in the present UCAMM. If the layers were secondary products on the Antarctic snow, similar layers should be found in other micrometeorites. The layers are also distinct from the magnetite rim at the surface of micrometeorites formed during heating by atmospheric entry and oxidation (Toppani et al., 2001).

Sodium, K, and Cl are uniformly observed in the smooth region and sporadically observed in the globular region (Fig. 9). Halite was also identified by XRD (see electronic supplementary data, S3). Although it is difficult to evaluate whether they are indigenous or terrestrial contamination, the homogeneous distributions of these elements, as well as N and S, do not suggest crystal particles of sea salts. The globular region contains a grain consisting of O, Mg, and Si (Fig. 9b). A high-resolution TEM image of the grain shows that the grain is a polycrystalline aggregate of tiny crystals. By considering that O, Mg, and Si are major elements, 0.46- and 0.24-nm lattice fringes could be assigned as the lattice spacing of (200) (~0.46 nm) and (002) (~0.25 nm) of clinoenstatite (Fig. 9c).

3.2.5. Isotopic compositions

We found no isotopic hot spots in the organic matter in the UCAMMs (Fig. 10). The H, C, and N isotopic ratios of the UCAMM D05IB80 are in the range of terrestrial values and not clearly distinguished from those of epoxy ($<2\sigma_{OM} + 3\sigma_{epoxy}$). We conclude that the H, C, and N isotopic compositions are at the same levels as those of terrestrial organics (Fig. 10).

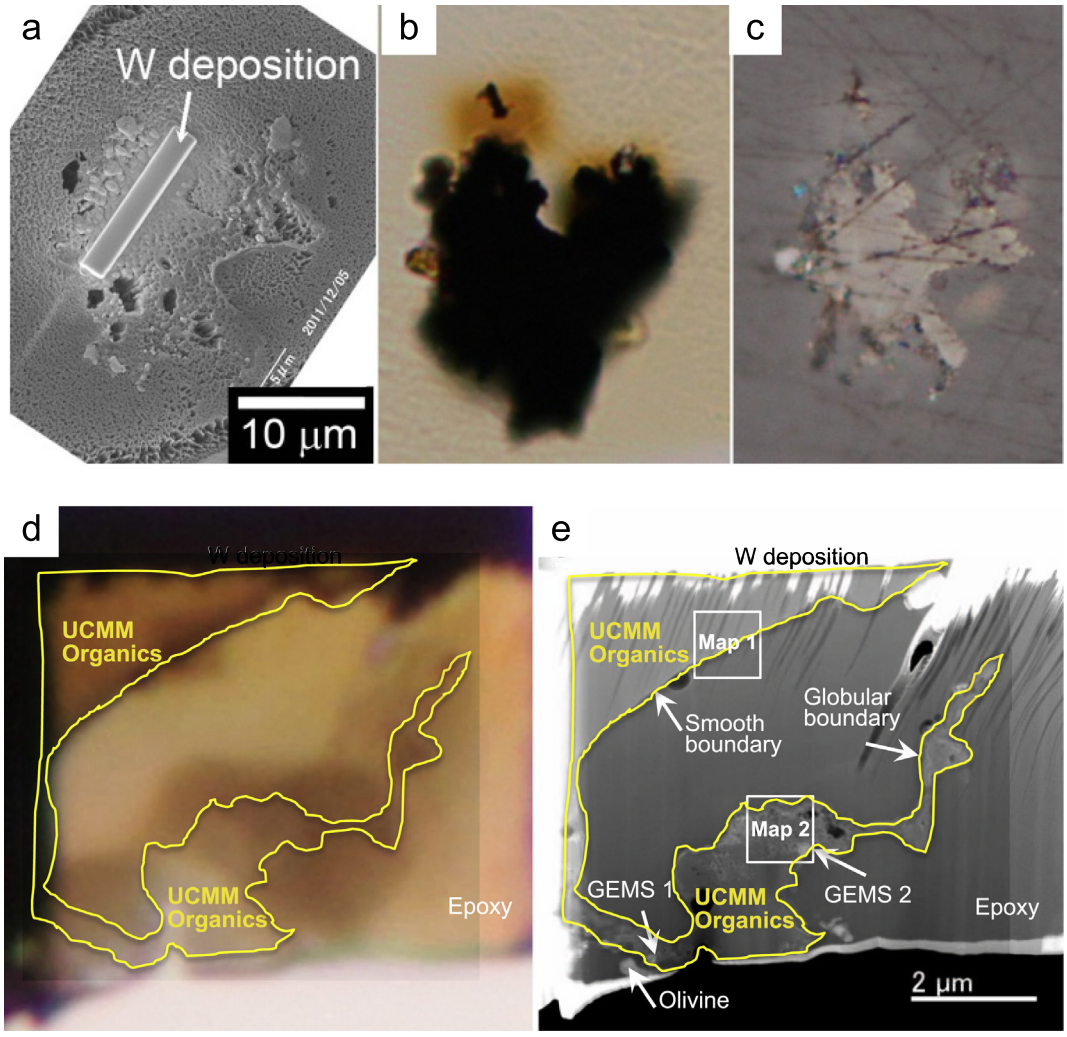

Fig. 5. (a) Back-scattered electron image, (b) optical image by a transmitted light, and (c) optical image by a reflected light of the surface of the polished cross-section of the UCAMM D05IB80. The tungsten deposition shown in (a) is the position where the focused ion beam (FIB) section was lifted out. (d) Transmitted optical image of the FIB section of the UCAMM D05IB80. The dark-brown and the light-brown areas are in contact along a sinuous boundary. (e) High-angle annular dark-field scanning transmission electron microscopy (HAADF-STEM) image of the FIB section of D05IB80, in which parallel grooves running from upper right to lower left are tracks formed by Cs^+ ion implantation during the SIMS mapping analysis. The two morphologies (smooth and globular) are indicated by arrows. Two box areas indicate where elemental mapping and high-resolution observation were performed (Fig. 9). Two GEMS grains and a polycrystalline olivine are also indicated.

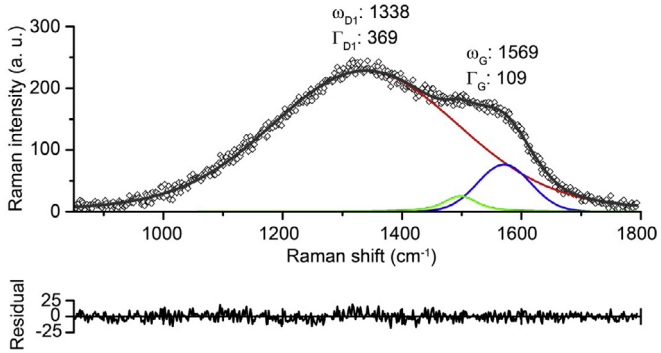

Fig. 6. Raman spectrum of the organic material in the UCAMM D05IB80. Background was subtracted. Peak position and full width at the half maximum (FWHM) of D_1 and G bands are shown as ω_{D1}, Γ_{D1}, ω_G, and Γ_G, respectively. In this spectrum, D_1 (red line), D_2 (green line), and G (blue line) bands were used to fit the spectrum. The residual graph is the difference between the raw spectrum and the fitted spectrum. (For interpretation of the references to colour in this figure legend, the reader is referred to the web version of this article.)

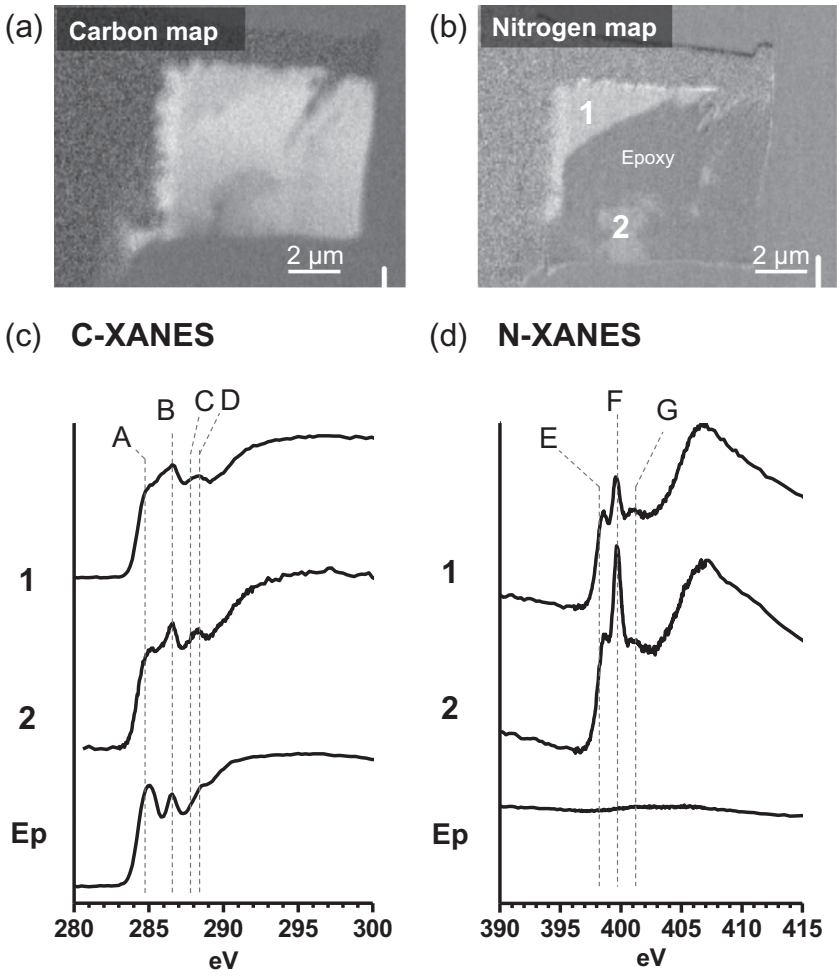

Fig. 7. (a) Carbon and (b) nitrogen distribution maps of the UCAMM D05IB80 obtained by STXM, and (c) carbon and (d) nitrogen XANES spectra of the regions 1, 2, and the epoxy indicated in (b). Peak assignments are based on Leinweber et al. (2007) and Cody et al. (2008); peak A: 1s-π^* transition for aromatic carbon (C═C*) at 285.1 eV, peak B: 1s-π^* transition for N-heterocycles (C─N*═C), nitrile (C≡N*) or vinyl-keto carbon (C═C─C*═O) at ~286.6 eV, peak C: 1s-3p/s* transition for aliphatic carbon at CHx-C at ~287.5 eV, peak D: 1s-π^* transition for carbonyl carbon in amide (NHx(C*═O)C) at ~288.0–288.2 eV and/or 1s-π^* transition for carbonyl carbon in carboxyl or ester (OR(C*═O)C) at ~288.4–288.7 eV, peak E: 1s-π^* transition for imine (C═N*) at 398.8 eV, peak F: 1s-π^* transition for N-heterocycles (C─N*═C) and/or nitrile (C≡N*) at ~399.7 eV, and peak G: 1s-π^* transition for amide (N*Hx(C═O)C) or 1s-3p/s* transition for amino (C─N*Hx) at 401.5 eV.

4. DISCUSSION

4.1. Primitive nature of UCAMM organics

The highly resolved N-XANES spectra of UCAMM D05IB80 are significantly different from the less characteristic, low signal-to-noise N-XANES spectra of insoluble organic macromolecules (IOM) from chondritic organic materials (e.g. Cody et al., 2008). According to the spectral fitting, the ratio of nitrogen to carbon in the smooth region of the UCAMM organics (N/C = ~0.15) is five times higher than that of insoluble organic macromolecules in types 1 and 2 chondritic meteorites (N/C = ~0.03, Alexander et al., 2007) (Fig. 11). The high nitrogen abundance and most of the identified functional groups (imine C═N, aromatic nitrogen heterocycles C─N═C, nitrile C≡N, amide NHx(C═O)C, and carbonyls COOR) indicate that the UCAMM organic material has high polarity, which indicates its hydrophilic nature and is consistent with the fact that the organic soluble phase was dissolved into epoxy (*i.e.*, polar solvent) (Fig. 5).

In prebiotic organic chemistry, *any* materials become insoluble, tar-like, hydrophobic macromolecules when energy is continuously provided to the molecules (Benner et al., 2012). Considering this general chemical phenomenon, the nitrogen- and oxygen-bearing polar functional group compositions and the solvent solubility indicate that the UCAMM organic material is extremely primitive compared to those in carbonaceous chondrites.

4.2. Formation of UCAMM organics and the role of small degree of aqueous alteration

Nitrogen-rich and oxygen-bearing complex organic molecules have been synthesized by UV photolysis of ices with simulated interstellar/precometary compositions (e.g.

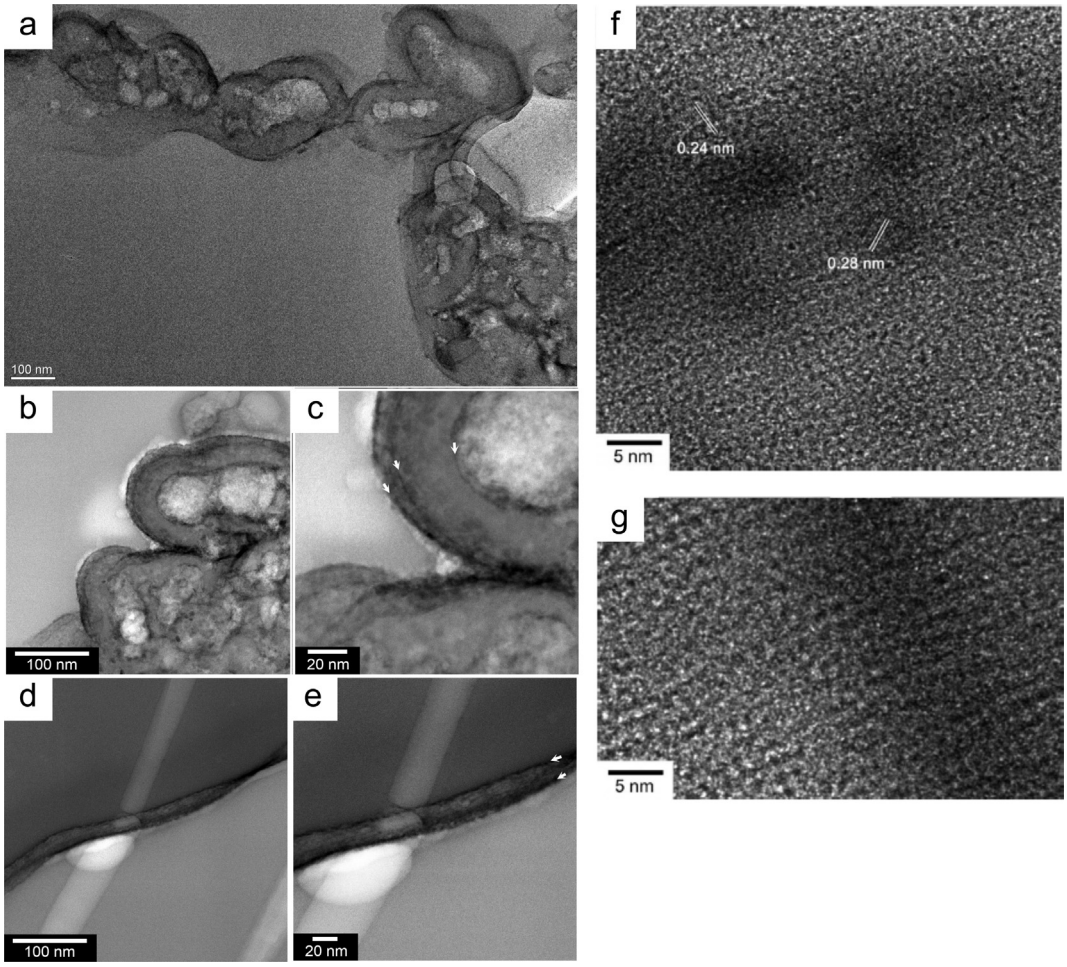

Fig. 8. (a) BF TEM images obtained by *in-situ* observation of organic nanoglobules in the UCAMM D05IB80. (b) Moderate- and (c) high-resolution BF TEM images of the globular boundaries. (d) Moderate- and (e) high-resolution BF TEM images of the smooth boundary. Thin (<2 nm) less-electron transparent layers indicated by arrows exist on both kinds of boundaries shown in (c) and (e). (f) High-resolution TEM image of the thin layer in the globular boundary shows nanocrystals indicating 0.24- and 0.28-nm lattice fringes. (g) High-resolution TEM image of the thin layer in the smooth region shows that there are no nanocrystals in the boundary.

H_2O, CH_3OH, CO, NH_3) (e.g. Bernstein et al., 1995; Dworkin et al., 2001; Nuevo et al., 2011), and they were mostly soluble and/or oily (Bernstein et al., 1995; Dworkin et al., 2001; Nuevo et al., 2011), having nanoglobule-like vesicles (Dworkin et al., 2001). The UCAMM in this study has a chemical similarity to the synthesized organics; the UCAMM contains functional groups of nitrile, imine, and amide (Fig. 7d), which were also observed in the photochemical product of Nuevo et al. (2011). The photochemical reaction of ices in interstellar or pre-stellar environments may have played a role in forming the organic macromolecules in the UCAMM, but the XANES spectrum of the experimentally synthesized organic matter is not completely the same as that of the present UCAMM. Furthermore, the bulk N/C (=0.28) and O/C (=0.51) ratios of the synthesized materials (Nuevo et al., 2011) are much higher than those of the UCAMM. Therefore, photochemistry alone could not be the process responsible for the formation of UCAMM and an additional process(es) would be necessary.

Here, we propose that very weak aqueous alteration in the parent body of the UCAMM was responsible for the chemical, structural, mineralogical, and morphological characteristics of the UCAMM. The accretion of organics, ice, and submicron-size mineral particles is a necessary process for the formation of a cometary body of sufficient size to retain liquid water, i.e., a meter- to kilometer-size object. In a comet, short-term heating, such as by planetesimal shock, could locally melt ice grains and release water, which could dissolve organic material. Unlike meteorite parent bodies in which aqueous fluid mobilizes due to high thermal conductivity with compact mineral structure, it is improbable that aqueous fluid mobilizes in a comet parent body due to the very low thermal conductivity of the porous ice structure (40–80% on average) (e.g., Kouchi et al., 1992; Asphaug and Benz, 1996; Farnham and Cochran, 2002; Kofman et al., 2015). Accordingly, the aqueous fluid on a porous icy body allows the formation of a large-size organic puddle.

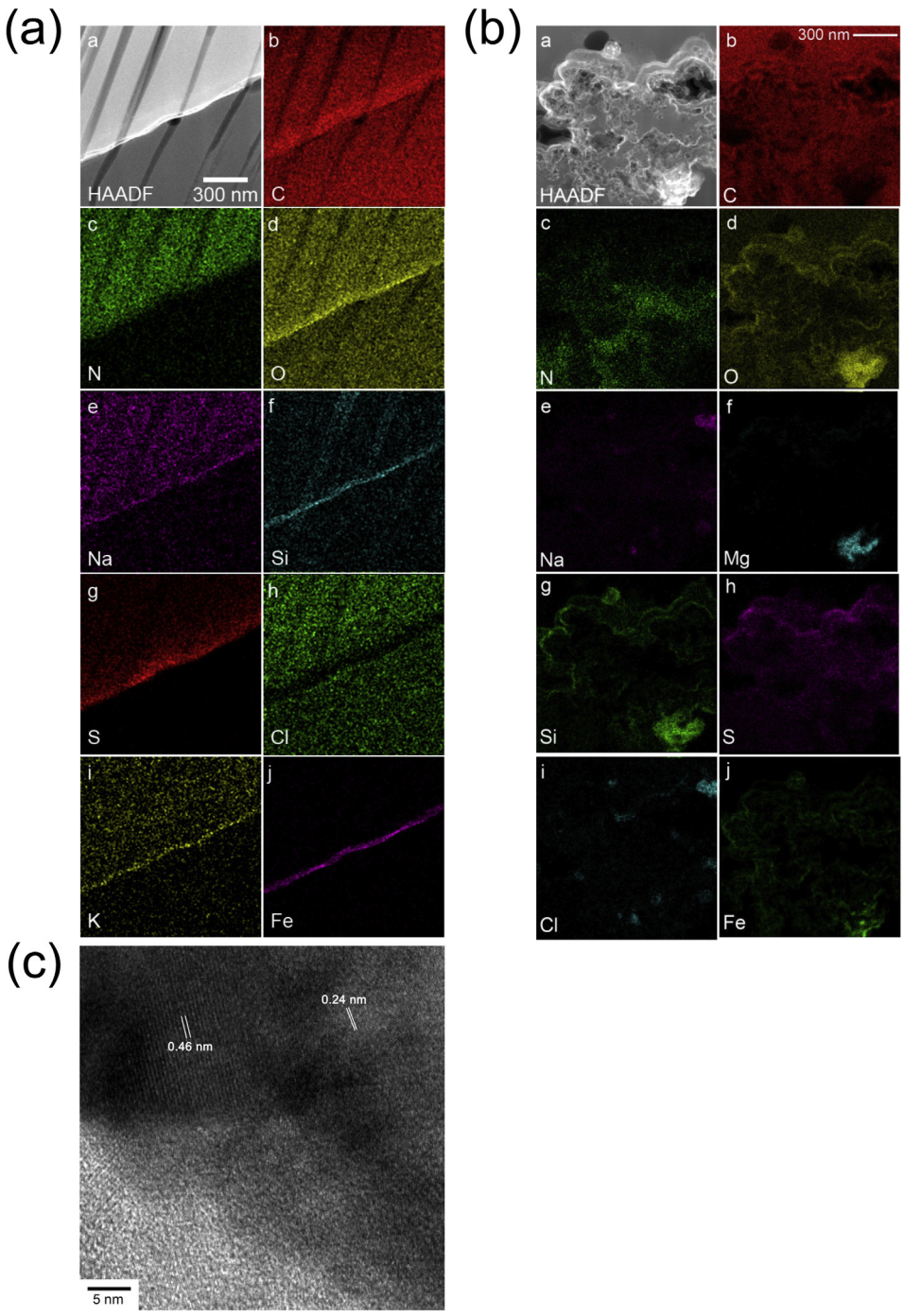

Fig. 9. (a) Elemental distribution maps of the smooth boundary shown as "Map 1" in Fig. 5e. The area near the boundary is enriched in C, O, Na, Si, S, K, and Fe. (b) Elemental distribution maps of the globular boundary shown as "Map 2" in Fig. 5e. The area near the boundary is enriched in C, O, Si, S, and Fe. The less electron transparent material is enriched in O, Si, S, and Fe. A GEMS grain appears as an O, Mg, and Si enriched area in the lower right corner. (c) High—resolution TEM image of a polycrystalline aggregate of tiny crystals included in a globule. The tiny crystals show 0.46- and 0.24-nm lattice fringes.

A very low degree of melting of ice in a comet or an icy planetesimal, causing low mobilization of the fluid, well explains the following observations in the present study.

(i) *Sulfurization of organics.* UCAMM D05IB80 contains a considerable amount of sulfur, the source of which is easily explained if it was formed in a comet or an icy body. H_2S is a typical component of cometary volatiles (Bockelée-Morvan et al., 2004) and also an aqueous alteration product of sulfide. Thus, the icy parent body of UCAMM D05IB80 may have contained it. Nucleophilic attack of H_2S could have

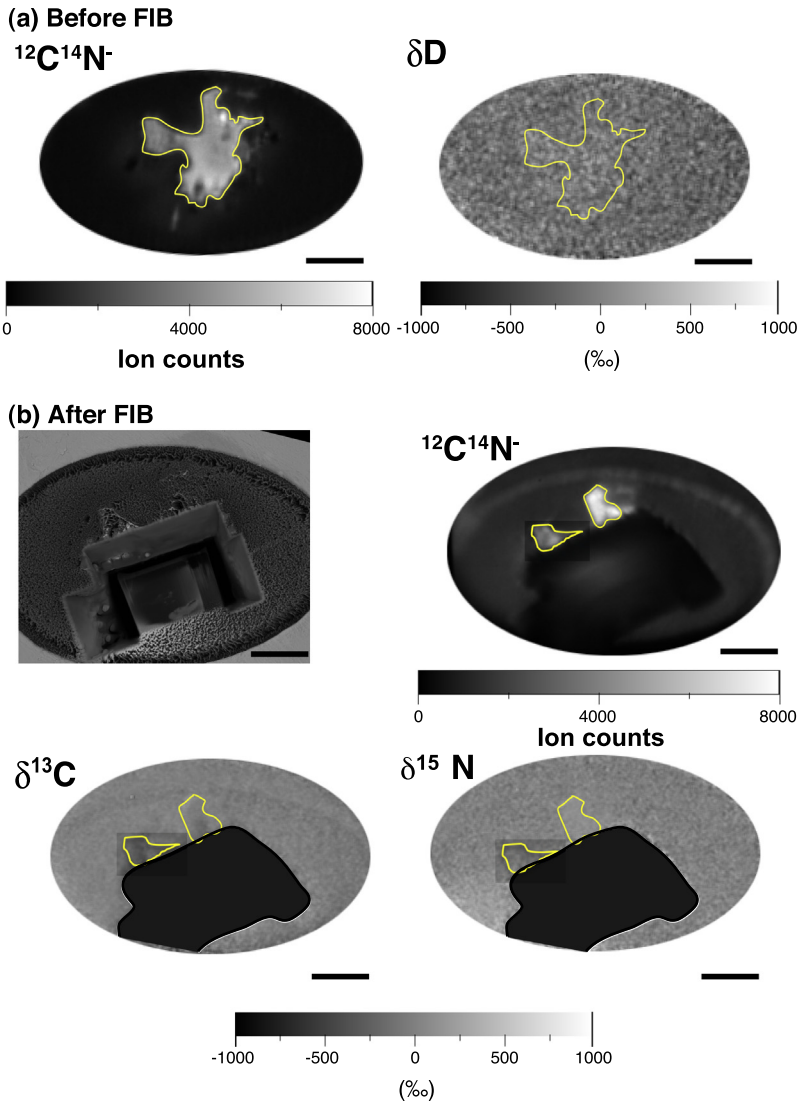

Fig. 10. (a) The $^{12}C^{14}N^-$ and δD isotopographs before preparing an FIB thin section. Scale bars are 10"μm. Color bars are secondary ion counts for the $^{12}C^{14}N^-$ isotopograph and isotope ratio with delta value for the δD isotopograph. (b) BSE image, $^{12}C^{14}N^-$, $\delta^{13}C$, and $\delta^{15}N$ isotopographs after making the FIB thin section. Scale bars are 10 μm. Color bars are secondary ion counts for the $^{12}C^{14}N^-$ isotopograph and isotope ratio with delta value for the $\delta^{13}C$ and $\delta^{15}N$ isotopographs. (For interpretation of the references to colour in this figure legend, the reader is referred to the web version of this article.)

taken place on the partially positive carbonyl carbon of the UCAMM organics (Fig. 7c) and/or their precursor molecule in aqueous fluid. For instance, ketones and aldehydes experimentally gave high yields of organic sulfides (R-S_x-R′) via a reaction with reduced inorganic sulfur (e.g., HS^-) in aqueous solution at relatively low temperature (20–50 °C) in short-durations (e.g. 22 h to 4 weeks) (Schouten et al., 1994; van Dongen et al., 2003).

(ii) *Formation of inorganic nanolayers at the surface of organic material.* The organics in UCAMM D05IB80 are covered with a thin inorganic layer, as shown in Fig. 8, which can be explained by the adsorption of mineral nanoparticles to an ice–fluid interface. When a fluid is frozen, a partition imbalance of anions and cations between ice and liquid occurs and is relaxed by the transfer of H^+ and OH^- to each phase, resulting in disproportionate pH between the two phases (Watanabe et al., 2014). The ion-transfer current changes at the interface between organics and salt-bearing ice (Qu et al., 2015). At the interface of two phases with a strong contrast of pH and redox potential, silicate and sulfide membranes osmotically precipitate from the dissolved ions in a fluid (Cairns-Smith, 1982; Russell et al., 1994). The interaction of particles at the ice–fluid interface occurs instantaneously at a cooling rate of –10 to –15 K/min from room temperature (Körber et al., 1985). The organic nanoglobules in the Tagish Lake meteorite display similar layers that

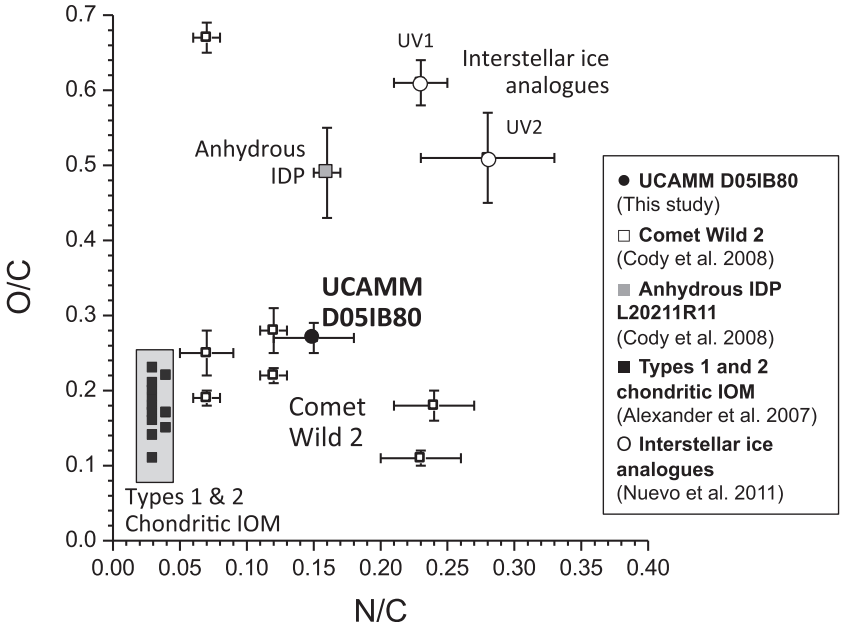

Fig. 11. N/C versus O/C ratios of organics in the UCAMM D05IB80 (●, this study), the comet Wild 2 dust particles (□, Cody et al., 2008), the anhydrous IDP L20211R11 (■, Cody et al., 2008), types 1 and 2 chondritic insoluble organic solids (■, Alexander et al., 2007), and the UV irradiation products from interstellar analogues (O, Nuevo et al., 2011) (UV1 H_2O:CH_3OH:CO:NH_3 = 100:50:1:1, UV2 H_2O:CH_3OH:CO:NH_3:C_3H_8 = 100:50:1:1:10). The ratios were estimated from the fitting of C-, N-, and O-XANES spectra.

contain predominantly carbon with minor amounts of O, Si, S, Cl, and Fe (Nakamura et al., 2002), which may also be due to the behaviors of ions and mineral particles in a frozen aqueous environment of its parent body.

(iii) *Formation of irregularly shaped nanoglobule aggregates.* The organics in UCAMM D05IB80 show different textures (smooth and globular textures) (Fig. 8), but their similar chemical compositions suggest simultaneous formation from a common precursor material (Fig. 7). The organic nanoglobules, which would have been round originally, deformed in shape (e.g. budding) via a pH gradient and/or change of osmotic pressure caused by the generation of a small amount of fluid. For instance, the charge state of an organic molecule changes under different pH, as exemplified by a protonated carboxylic acid (R-COOH) at lower pH and an ionized carboxylate ($R\text{-}COO^-$) at higher pH. Vesicles are produced at around neutral pH, at which the molar ratio of the protonated and ionized forms is equal (e.g. Nawa et al., 2013). However, the fluid in a cometary body could be basic because of the redistribution of ions (Watanabe et al., 2014) and/or high concentration of NH_3 (Nakamura-Messenger et al., 2011). At high pH, the vesicles are rapidly deformed (in several seconds) due to the dissolution of an ionized form (Nawa et al., 2013). Similarly, textural variations of nanoglobules in insoluble organic residues (De Gregorio et al., 2013; Changela et al., 2013) and matrices (Ivuna, Orgueil and Tagish Lake, see electronic supplementary data S4) from aqueously altered carbonaceous chondrites imply exposure to basic fluid that was generated through the formation of phyllosilicates during aqueous alteration on their meteorite parent bodies.

4.3. Mineralogical evidence of small degree of aqueous alteration

Although the GEMS grains in D05IB80 contain tiny crystals of Fe-Ni metal and Fe sulfide (Fig. 2), they are rarer than those in GEMS in CP IDPs (e.g. Keller and Messenger, 2011) and CP MMs (Noguchi et al., 2015). Mg in the amorphous silicate in GEMS grains is heterogeneously distributed and on average highly depleted (Fig. 2c). By contrast, Si is enriched in the Mg-depleted areas in GEMS (Fig. 2c). The heterogeneous distribution of Si and Mg within each GEMS grain in IDPs has already been reported (e.g. Keller and Messenger, 2011). In the case of D05IB80, Si-rich areas are predominant and amorphous silicate is enriched in Fe (Figs. 2 and 3).

Because Fe-Ni metal is among the first phases to alter by aqueous alteration (Zolensky et al., 1993; Hanowski and Brearley, 2000, 2001; Chizmadia et al., 2008), the rarity of nano Fe metal in GEMS indicates a slight degree of aqueous alteration. It has already been reported that rare Fe-Ni metal phases were found in the UCAMMs and their GEMS-like objects collected by the French–Italian team (Dobrică et al., 2012). The depletion of metal may be a common feature of UCAMMs. The GEMS grains with rare nanophase Fe metal particles in the Acfer 094 carbonaceous chondrite (Vollmer et al., 2009a, 2009b) have been thought to be the result of oxidation of Fe metal due to nascent aqueous alteration of the amorphous silicates (Keller

et al., 2009). Le Guillou and Brearley (2014) reported the absence of metal grains associated with amorphous silicate material in the MET 00426 CR3 chondrite and discussed that the absence was due to hydration of the amorphous silicate.

In the case of D05IB80, nano Fe sulfide is also depleted in GEMS. However, this does not necessarily mean that D05IB80 experienced slightly higher degrees of aqueous alteration than primitive meteorites because hydrous phyllosilicates are not identified in the UCAMM. A slightly oxidizing condition of aqueous alteration might have promoted the dissolution of nano Fe sulfide in the GEMS of the UCAMM.

There is no Ni-bearing pyrrhotite in the UCAMM (<3.2 at% Ni) (Fig. 3d), which is consistent with the idea that the UCAMM experienced very weak aqueous alteration. A minimal degree of aqueous alteration is also consistent with aqueous alteration products not being found on olivine and pyroxene (Fig. 6).

Based on the chemical and mineralogical features described above, we conclude that the UCAMM experienced a very weak degree of aqueous alteration on a cometary nucleus or icy asteroid, which is not seen on the typical types 1 and 2 chondritic meteorite parent bodies. Possible heat sources for the generation of liquid water in icy small bodies include (i) short-lived radioactive nuclides, (ii) perihelion passage (Nakamura-Messenger et al., 2011), (iii) collisions of planetesimals (Cody et al., 2011), and (iv) reduction of the freezing point by the presence of solutes, e.g. ammonia (Pizzarello et al., 2011) or methanol.

The condition of aqueous alteration of the UCAMM can be estimated by the experiments by Nakamura-Messenger et al. (2011). They conducted a hydrothermal experiment on anhydrous IDPs and reported rapid formation of hydrated silicates at 25–160 °C for 12–24 h under basic pH conditions (pH = 12), that is, the alteration of amorphous silicate into hydrous phyllosilicate may proceed extremely quickly. UCAMM D05IB80 does not contain hydrous silicates; Mg and S leached out from GEMS grains instead, which indicates a shorter duration reaction at lower temperature, lower pH, and/or slightly oxidizing conditions compared to the experiments. Considering that the degree of alteration should have been much lower than the aqueous alteration in the major CM and CI carbonaceous chondrites, which lasted for several million years (e.g. Fujiya et al., 2013), planetesimals collisions are most likely cause to produce a very weak degree of aqueous alteration in a short duration. The large $P\Delta V$ irreversible energy deposition during the compaction of pore spaces of cometary ices initiates melting at the very low shock pressures of 0.1–0.5 GPa between 250 and 150 K (Stewart and Ahrens, 2004). The pressure range is comparable to that of typical impact velocities of comets, which generate peak pressures of ~1 GPa (Stewart and Ahrens, 2004).

Although there may be a possibility that the UCAMM suffered terrestrial weathering in Antarctic snow, this possibility would be low because iron hydroxide, which is easily formed by the weathering of pyrrhotite (Taylor et al., 2002), was not identified. The residence time of micrometeorites in Antarctic snow is much shorter (ca. a year) than the lifetime of Antarctic ice (ca. thousands years), and the average temperature near the Dome Fuji Station is −54°C (Shiraishi, 2012), which would prevent the weathering reaction.

4.4. Comparison with other UCAMMs, AMMs, IDPs, comets, and chondritic meteorites

UCAMM D05IB80 consists of large (tens of micrometers) organic material with submicron-sized mineral species, such as crystalline silicate, sulfide, and GEMS grains. Similarly, the UCAMMs investigated by Duprat et al. (2010) and Dobrică et al. (2012) have continuous large areas composed of carbonaceous material, and minerals and GEMS grains are embedded in the carbonaceous material. The nitrogen chemical characteristics of the organic material in UCAMM D05IB80 is consistent with those described by Dartois et al. (2013), who identified C=N and C≡N from their non-FIB UCAMM samples. The similarity suggests that the organic chemistry and mineralogy identified in the present study are common for UCAMMs, although GEMS grains in their UCAMMs are enriched in Fe sulfide nanocrystals and do not show depletion of Mg and S.

The isotopic compositions of UCAMMs appear to be highly variable, but the D, ^{13}C, and ^{15}N isotopic compositions in this study are normal, which is also the case for a UCAMM containing abundant presolar grains (Floss et al., 2012). On the contrary, extreme enrichments of D and ^{15}N were found in two UCAMMs by the French–Italian team (Duprat et al., 2010; Dartois et al., 2013). Duprat et al. (2010) showed that one UCAMM had an area of larger D excess ($\delta D > \sim 10000‰$) than another ($\delta D > 5400‰$) with a clear boundary. Indeed, the stratosphere IDPs (Messenger, 2000) and the comet Wild 2 dust particles (Matrajt et al., 2012) show a wide range of H and N isotopic compositions, from values extremely rich in heavy isotopes to normal values with the terrestrial levels. Thus, it is difficult to determine the origin of the samples by only the presence or absence of the isotopic anomalies.

The anhydrous interplanetary dust particle (IDP) L2006LB23 is comprised mainly of carbonaceous material (~90%) (Thomas et al., 1994). The IDP is regarded as an ultracarbonaceous IDP. The ultramicrotomed section (Figs. 1 and 2 in Thomas et al., 1994) has a bubble-wall structure made by organic material containing minerals grains, which is quite similar to the sections of the UCAMM D05IB80. Both the internal structure and also the mineralogy of the ultracarbonaceous IDP are similar to those of the UCAMM D05IB80. The IDP contains Si-rich glass containing Fe sulfide and Fe-Ni metal grains, Si-rich glass, pyroxene, olivine, and Fe sulfide. In addition to pyroxene, olivine, and Fe sulfide, the UCAMM D05IB80 contains amorphous SiO_2 and GEMS grains that are highly depleted in Mg and S (Figs. 2 and 3). It is likely that these two phases correspond to the Si-rich glass and Si-rich glass containing Fe sulfide and Fe-Ni metal grains in L2006LB23. These data suggest that there is a genetic relationship between these objects.

The mineralogy and nitrogen-rich organic functional group chemistry of the UCAMM D05IB80 are in common with those of one of the anhydrous AMMs (D10IB009) col-

lected from the Antarctic snow near the Dome Fuji Station (Noguchi et al., 2017). On the other hand, a difference is that D10IB009 contains GEMS including Fe-metal, thus it is likely that the UCAMM D05IB80 is aqueously more altered than the anhydrous AMM. Another difference is that the organic material in D10IB009 has D- and ^{15}N-enrichments ($\delta D = \sim 2000–10{,}000‰$, $\delta^{15}N = \sim 300–1000‰$) (Noguchi et al., 2017), similarly to CP-IDPs (e.g., Messenger, 2000), although it is unlikely that the lack of isotopic anomalies in the UCAMM is due to the aqueous alteration, based on the fact that a number of aqueously altered carbonaceous chondrites retain organics enriched in heavy isotopes (e.g. Busemann et al., 2006; Nakamura-Messenger et al., 2006; Hashiguchi et al., 2013).

It should be noted that the N-XANES spectra of regions 1 and 2 in the UCAMM D05IB80 (Fig. 7d) are very similar to those of three particles from comet Wild 2 with N/C ratios of 0.08–0.16, one of which was an organic nanoglobule with a nitrogen isotopic composition indistinguishable from terrestrial values (De Gregorio et al., 2010). Other particles of comet Wild 2 have lesser amounts of imine, nitrile, and amidyl groups than amino, urea, and carbamoyl (NHx(C═O)OR) groups in their N-XANES spectra (Cody et al., 2008), but the N/C (~0.12) and O/C (0.22–0.28) ratios of some of the spectra are comparable to those in this study (Fig. 11). Moreover, the appearance of the organic soluble phase in UCAMM D05IB80 extracted from epoxy (Fig. 5) is similar to those of the epoxy-soluble organic matter in the comet Wild 2 dust particles (Cody et al., 2008; De Gregorio et al., 2011).

The chemical and isotopic characteristics of the UCAMM D05IB90 are significantly different from those of the organic materials in types 1 and 2 carbonaceous chondrites (e.g. Cody et al., 2011), but they are similar to those of some of the primitive CR3 chondrites. The large smooth organic material connected with globular organics in the UCAMM is similar to that in the CR3 chondrite MET 00426 observed by Le Guillou and Brearley (2014), which is an elongated vein with a length of 3–4 μm and a width up to 1 μm, with a sharp boundary between surrounding silicates and sulfides. They observed a single organic nanoglobule embedded in the main organic mass and an aggregate of rounded particles connected to the main vein. Peeters et al. (2012) also found a several-micron-sized organic vein containing a number of nanoglobules in the QUE 99177 CR3 chondrite, which has an N-XANES spectrum similar to that of our observation. The comet Wild 2 is estimated to have experienced little or no aqueous alteration based on the absence of phyllosilicates (Zolensky et al., 2006). CR3 chondrites contain an abundance of amorphous silicates (e.g. Abreu and Brearley, 2010; Le Guillou and Brearley, 2014) and are thought to have experienced the earliest stage of parent body aqueous alteration. Therefore, the similarities among the organics in the UCAMM D05IB80, the comet Wild 2, and CR3 chondrites corroborate that the UCAMM is more primitive than most of the aqueously altered carbonaceous chondrites.

The recent Visible, Infrared and Thermal Imaging Spectrometer (VIRTIS) results from the Rosetta mission revealed the presence of an organic-rich, dark, dehydrated surface on the comet 67P/Churyumov-Gerasimenko (Capaccioni et al., 2015). The evolved gas analyzer Cometary Sampling and Composition (COSAC) mass spectrometer identified a number of nitrogen-bearing organic molecules, such as nitriles, amines, amides, and isocyanates, but no sulfur species on the comet 67P/C-G (Goesmann et al., 2015). The high abundance and chemical compositions of organics on 67P/Churyumov-Gerasimenko may be related to the precursor material of the large N-rich organics of the UCAMM, prior to organic sulfurization under an aqueous condition.

Moreover, our work reports the first finding of organic materials from micrometeorites retaining the elements C, H, O, N, and S all together. Another finding of CHONS organics has been reported from the polar solvent extracts from the Murchison meteorite (Schmitt-Kopplin et al., 2010). Because of the unusual similarity of organic elemental compositions and polar nature between the UCAMM and the Murchison, the possibility that the UCAMM organics contain the precursor of the meteoritic CHONS compounds is expected, and it could be a key indicator of the comet-asteroid continuum. In order to trace back and determine the precursors of organic materials in the early solar system, further analyses and comparative studies of the most primitive extraterrestrial materials that we can obtain—such as anhydrous micrometeorites, IDPs, and the least altered carbonaceous chondrites—through comprehensive inorganic and organic analytical strategies without discrimination between soluble and insoluble will be necessary.

5. SUMMARY

An ultracarbonaceous micrometeorite (UCAMM D05IB80), collected from near the Dome Fuji Station, Antarctica, was investigated by coordinated *in-situ* analyses. According to the following unique features of the organics and minerals, which are different from those of chondritic meteorites, we conclude that the UCAMM formed by a small amount of fluid-induced interaction of organics and minerals in a porous ice-rich cometary body.

1. A major part of the organic materials in the UCAMM shows a smooth texture to which globular aggregates are connected and includes an epoxy-soluble phase. The UCAMM shows nitrogen-rich organic chemistry (N/C = 0.15). Its organic functional groups include a variety of nitrogen-bearing groups: heterocyclic nitrogen, nitrile, imine, and amide. The polar functional group compositions and the solvent solubility indicate a very primitive nature of the organic material in the UCAMM.
2. The GEMS grains are depleted in Mg and S. This is evidence for incipient aqueous alteration in the UCAMM parent body. Shock heating in an icy planetesimal instantaneously melted ice grains and released water, which dissolved organic material. Due to the high porosity and low density of a cometary body, the fluid did not diffuse but rather formed a large-size organic puddle

(15×15 μm). The locally generated fluid sulfurized organic material, formed thin mineral layers (C, O, Si, S, and Fe) at the surface of organics, and deformed the shape of organic nanoglobules.

ACKNOWLEDGEMENTS

We appreciate Christine Floss, an anonymous reviewer, and associate editor Eric Quirico for their constructive comments and helpful editorial handling. This work was supported by a Grant-in-Aid for Scientific Research from the Japanese Ministry of Education, Culture, Sports, Science and Technology (No. 22224010, PI: H. Nagahara). The STXM facility at the beamline 5.3.2.2, ALS, is supported by the Department of Energy, Basic Energy Sciences Program.

APPENDIX A. SUPPLEMENTARY MATERIAL

Supplementary data associated with this article can be found, in the online version, at http://dx.doi.org/10.1016/j.gca.2017.06.047.

REFERENCES

Abreu N. M. and Brearley A. J. (2010) Early solar system processes recorded in the matrices of two highly pristine CR3 carbonaceous chondrites, MET 00426 and QUE 99177. *Geochim. Cosmochim. Acta* **74**, 1146–1171.

Alexander C. M. O'. D., Fogel M., Yabuta H. and Cody G. D. (2007) The origin and evolution of chondrites recorded in the elemental and isotopic compositions of their macromolecular organic matter. *Geochim. Cosmochim. Acta* **71**, 4380–4403.

Asphaug E. and Benz W. (1996) Size, density, and structure of comet shoemaker-Levy 9 inferred from the physics of tidal breakup. *Icarus* **121**, 225–248.

Bassim N. D., De Gregorio B. T., Kilcoyne A. L. D., Scott K., Chou T., Wirick S., Cody G. and Stroud R. M. (2012) Minimizing damage during FIB sample preparation of softmaterials. *J. Microscopy* **245**, 288–301.

Benner S. A., Kim H.-J. and Carrigan M. A. (2012) Asphalt, water, and prebiotic synthesis of ribose, ribonucleosides, and RNA. *Acc. Chem. Res.* **45**, 2025–2034.

Bernstein M. P., Sandford S. A., Allamandola L. J., Chang S. and Scharberg M. A. (1995) Organic compounds produced by photolysis of realistic interstellar and cometary ice analogs containing methanol. *Astrophys. J.* **454**, 327–344.

Bockelée-Morvan D., Crovisier J., Mumma M. J. and Weaver H. A. (2004) The composition of cometary volatiles. In *Comets II* (eds. M. C. Festou, H. U. Keller and H. A. Weaver). The University of Arizona Press, Tucson, AZ, pp. 391–423.

Bradley J. P. and Brownlee D. E. (1986) Cometary particles: thin sectioning and electron beam analysis. *Science* **231**, 1542–1544.

Bradley J. P. and Dai Z. R. (2004) Mechanism of formation of glass with embedded metal and sulfides. *Astrophys. J.* **617**, 650–655.

Bradley J. P., Keller L. P., Snow T. P., Hanner M. S., Flynn G. J., Gezo J. C., Clemett S. J., Brownlee D. E. and Bowey J. E. (1999) An infrared spectral match between GEMS and interstellar grains. *Science* **285**, 1716–1718.

Busemann H., Young A. F., Alexander C. M. O'. D., Hoppe P., Mukhopadhyay S. and Nittler L. R. (2006) Interstellar chemistry recorded in organic matter from primitive meteorites. *Science* **314**, 727–730.

Busemann H., Nguyen A. N., Cody G. D., Hoppe P., Kiloyne A. L. D., Stroud R. M., Zega T. J. and Nittler L. R. (2009) Ultraprimitive interplanetary dust particles from the comet 26P/Grigg–Skjellerup dust stream collection. *Earth Planet. Sci. Lett.* **288**, 44–57.

Cairns-Smith A. G. (1982) *Genetic takeover and the mineral origins of life*. Cambridge University Press, Cambridge, England.

Capaccioni F., Coradini A. and Filacchione G., et al. (2015). *Science* **349**, aab0628-1- aab0628-4.

Changela H. G., Cody G. D., Alexander C. M. O'D., Nittler L. R., Peeters Z., De Gregorio B. T. and Stroud R. M. (2013) TEM Study of insoluble organic matter in primitive chondrites: Unusual textures associated with organic nanoglobules. *Lunar Planet. Sci.* **XLIV**, #3101.

Chizmadia L. J., Xu Y., Schwappach C. and Brearley A. J. (2008) Characterization of micron-sized Fe, Ni metal grains in fine-grained rims in the Y-791198 CM2 carbonaceous chondrite: Implications for asteroidal and preaccretionary models for aqueous alteration. *Meteor. Planet. Sci.* **43**, 1419–1438.

Cody G. D., Ade H., Alexander C. M. O'. D., Araki T., Butterworth A., Fleckenstein H., Flynn G., Gilles M. K., Jacobsen C., Kilcoyne A. L. D., Messenger K., Sandford S. A., Tyliszczak T., Westphal A. J., Wirick S. and Yabuta H. (2008) Quantitative organic and light-element analysis of comet 81P/Wild 2 particles using C-, N-, and O-XANES. *Meteor. Planet. Sci.* **43**, 353–365.

Cody G. D., Heying E., Alexander C. M. O. D., Nittler L. R., Kilcoyne A. L. D., Sandford S. A. and Stroud R. M. (2011) Establishing a molecular relationship between chondritic and cometary organic solids. *Proc. Natl. Acad. Sci. USA* **108**, 19171–19176.

Dartois E., Engrand C., Brunetto R., Duprat J., Pino T., Quirico E., Remusat L., Bardin N., Briani G., Mostefaoui S., Morinaud G., Crane B., Szwec N., Delauche L., Jamme F., Sandt Ch. and Dumas P. (2013) Ultracarbonaceous Antarctic micrometeorites, probing the Solar System beyond the nitrogen snowline. *Icarus* **224**, 243–252.

De Gregorio B. T., Stroud R. M., Nittler L. R., Alexander C. M. O'. D., Kilcoyne A. L. D. and Zega T. J. (2010) Isotopic anomalies in organic nanoglobules from Comet 81P/Wild 2: comparison to Murchison nanoglobules and isotopic anomalies induced in terrestrial organics by electron irradiation. *Geochim. Cosmochim. Acta* **74**, 4454–4470.

De Gregorio B. T., Stroud R. M., Cody G. D., Nittler L. R., Kilcoyne A. L. D. and Wirick S. (2011) Correlated microanalysis of cometary organic grains returned by Stardust. *Meteor. Planet. Sci.* **46**, 1376–1396.

De Gregorio B. T., Stroud R. M., Nittler L. R., Alexander C. M. O'. D., Bassim N. D., Cody G. D., Kilcoyne A. L. D., Sandford S. A., Milam S. N., Nuevo M. and Zega T. J. (2013) Isotopic and chemical variation of organic naoglobules in primitive meteorites. *Meteor. Planet. Sci.* **48**, 904–928.

Dobrică E., Engrand C., Quirico E., Montagnac G. and Duprat J. (2011) Raman characterization of carbonaceous matter in CONCORDIA Antarctic micrometeorites. *Meteor. Planet. Sci.* **46**, 1363–1375.

Dobrică E., Engrand C., Leroux H., Rouzaud J.-N. and Duprat J. (2012) Transmission electron microscopy of CONCORDIA ultracarbonaceous Antarctic micrometeorites (UCAMMs): mineralogical properties. *Geochim. Cosmochim. Acta* **76**, 68–82.

Duprat J., Dobrica E., Engrand C., Aléon J., Marrocchi Y., Mostefaoui S., Meibom A., Leroux H., Rouzaud J.-N., Gounelle M. and Robert F. (2010) Extreme deuterium excesses

in ultracarbonaceous micrometeorites from central Antarctic snow. *Science* **328**, 742–745.

Dworkin J. P., Deamer D. W., Sandford S. A. and Allamandola L. J. (2001) Self-assembling amphiphilic molecules: synthesis in simulated interstellar/precometary ices. *Proc. Natl. Acad. Sci. USA* **98**, 815–819.

Farnham T. L. and Cochran A. L. (2002) A McDonald observatory study of Comet 19P/Borrelly: placing the deep space 1 observations into a broader context. *Icarus* **160**, 398–418.

Floss C., Noguchi T. and Yada T. (2012) Ultracarbonaceous Antarctic micrometeorites: Origins and relationships to other primitive extraterrestrial materials. *Lunar Planet. Sci.* **XLIII**, #1217.

Floss C., Stadermann F. J., Bradley J., Dai Z. R., Bajt S. and Graham G. (2004) Carbon and nitrogen isotopic anomalies in an anhydrous interplanetary dust particle. *Science* **303**, 1355–1358.

Frank D. R., Zolensky M. E. and Le L. (2014) Olivine in terminal particles of Stardust aerogel tracks and analogous grains in chondrite matrix. *Geochim. Cosmochim. Acta* **142**, 240–259.

Fujiya W., Sugiura N., Sano Y. and Hiyagon H. (2013) Mn–Cr ages of dolomites in CI chondrites and the Tagish Lake ungrouped carbonaceous chondrite. *Earth Planet. Sci. Lett.* **362**, 130–142.

Garvie L. A. J. and Buseck P. R. (2004) Nanosized carbon-rich grains in carbonaceous chondrite meteorites. *Earth Planet. Sci. Lett.* **224**, 431–439.

Goesmann F., Rosenbauer H., Bredehoft J. H., Cabane M., Ehrenfreund P., Gautier T., Chaitanya Giri., Kruger H., Le Roy L., MacDermott A. J., McKenna-Lawlor S., Meierhenrich U. J., Munoz Caro G. M., Raulin F., Roll R., Steele A., Steininger H., Sternberg R., Szopa C., Thiemann W. and Ulamec S. (2015) Organic compounds on comet 67P/Churyumov-Gerasimenko revealed by COSAC mass spectrometry. *Science* **349**, aab0689-1- aab0689-3.

Greenberg J. M. and Li A. (1997) Silicate core-organic refractory mantle particles as interstellar dust and as aggregated in comets and stellar disks. *Adv. Space Res.* **19**, 981–990.

Hanowski N. P. and Brearley A. J. (2000) Iron-rich aureoles in the CM carbonaceous chondrites, Murray, Murchison and ALH81002: evidence for in situ alteration. *Meteor. Planet. Sci.* **35**, 1291–1308.

Hanowski N. P. and Brearley A. J. (2001) Aqueous alteration of chondrules in the CM carbonaceous chondrites, Allan Hills 81002. *Geochim. Cosmochim. Acta* **65**, 495–518.

Hashiguchi M., Kobayashi S. and Yurimoto H. (2013) In situ observation of D-rich carbonaceous globules embedded in NWA 801 CR2 chondrite. *Geochim. Cosmochim. Acta* **122**, 306–323.

Joswiak D. J., Brownlee D. E., Matrajt G., Westphal A. J. and Snead C. J. (2009) Kosmochloric Ca-rich pyroxenes and FeO rich olivines (Kool grains) and associated phases in Stardust tracks and chondritic porous interplanetary dust particles: possible precursors to FeO-rich type II chondrules in ordinary chondrites. *Meteorit. Planet. Sci.* **44**, 1561–1588.

Joswiak D. J., Brownlee D. E., Matrajt G., Westphal A. J., Snead C. J. and Gainsforth Z. (2012) Comprehensive examination of large mineral and rock fragments in Stardust tracks: mineralogy, analogous extraterrestrial materials, and source regions. *Meteorit. Planet. Sci.* **47**, 471–524.

Keller L. P. and Messenger S. (2011) On the origins of GEMS grains. *Geochim. Cosmochim. Acta* **75**, 5336–5365.

Keller L. P., Nakamura-Messenger K. and Messenger S. (2009) Amorphous silicates in primitive meteoritic materials: Acfer 094 and IDPs. 72nd Annual Meteoritical Society Meeting 44. #5371 (abstract).

Kilcoyne A. L. D., Tyliszczak T., Steele W. F., Fakra S., Hitchcock P., Franck K., Anderson E., Harteneck B., Rightor E. G., Mitchell G. E., Hitchcock A. P., Yang L., Warick T. and Ade H. (2003) Interferometer controlled scanning transmission microscopes at the advanced light source. *J. Synchrotron Rad.* **10**, 125–136.

Klöck W. and Stadermann F. J. (1994) Mineralogical and chemical relationships of interplanetary dust particles, micrometeorites and meteorites. In M. E. Zolensky, et al., (Eds.) Analysis of Interplanetary Dust. Dover, New York, pp. 51–87.

Kofman et al. (2015) Properties of the 67P/Churyumov-Gerasimenko interior revealed by CONSERT radar. *Science* **349**, aab0639-1 – aab0639-6.

Körber C., Rau G., Cosman M. D. and Cravalho E. G. (1985) Interaction of particles and a moving ice-liquid interface. *J. Cryst Growth* **72**, 649–662.

Kouchi A., Greenberg J. M., Yamamoto T. and Mukai T. (1992) Extremely low thermal conductivity of amorphous ice: relevance to comet evolution. *Astrophys. J.* **388**, L73–L76.

Le Guillou C. and Brearley A. J. (2014) Relationships between organics, water and early stages of aqueous alteration in the pristine CR3.0 chondrite MET00426. *Geochim. Cosmochim. Acta* **131**, 344–367.

Le Guillou C., Bernard S., Brearley A. J. and Remusat L. (2014) Evolution of organic matter in Orgueil, Murchison and Renazzo during parent body aqueous alteration: *In situ* investigations. *Geochim. Cosmochim. Acta* **131**, 368–392.

Leinweber P., Kruse J., Walley F. L., Gillespie A., Eckhardt K.-U., Blyth R. I. R. and Regier T. (2007) Nitrogen K-edge XANES – an overview of reference compounds used to identify 'unknown' organic nitrogen in environmental samples. *J. Synchrotron Rad.* **14**, 500–511.

Matrajt G., Messenger S., Brownlee D. and Joswiaki D. (2012) Diverse forms of primordial organic matter identified in interplanetary dust particles. *Meteor. Planet. Sci.* **47**, 525–549.

Matsumoto T., Tsuchiyama A., Nakamura-Messenger K., Nakano T., Uesugi K., Takeuchi A. and Zolensky M. E. (2013) Three-dimensional observation and morphological analysis of organic nanoglobules in a carbonaceous chondrite using X-ray microtomography. *Geochim. Cosmochim. Acta* **116**, 84–95.

Messenger S. (2000) Identification of molecular-cloud material in interplanetary dust particles. *Nature* **404**, 968–971.

Messenger S., Sandford S. and Brownlee D. (2006) The population of starting materials available for solar system construction. In *Meteorites and the early solar system II* (eds. D. S. Lauretta and , Jr.H. Y. McSween). Univ. of Arizona, USA, pp. 187–208.

Nakamura K., Zolensky M. E., Tomita S., Nakashima S. and Tomeoka K. (2002) Hollow organic globules in the Tagish Lake meteorite as possible products of primitive organic reactions. *Int. J. Astrobiol.* **1**, 179–189.

Nakamura T., Noguchi T., Ozono Y., Osawa T. and Nagao K. (2005) Mineralogy of ultracarbonaceous large micrometeorites. *Meteor. Planet. Sci.* **40**, A110.

Nakamura T., Noguchi T., Tanaka M., Zolensky M. E., Kimura M., Tsuchiyama A., Nakato A., Ogami T., Ishida H., Uesugi M., Yada T., Shirai K., Fujimura A., Okazaki R., Sandford S. A., Ishibashi Y., Abe M., Okada T., Ueno M., Mukai T., Yoshikawa M. and Kawaguchi J. (2011) Itokawa dust particles: a direct link between S-type asteroids and ordinary chondrites. *Science* **333**, 1113–1116.

Nakamura-Messenger K., Messenger S., Keller L. P., Clemett S. J. and Zolensky M. E. (2006) Organic globules in the Tagish Lake meteorite: remnants of the protosolar disk. *Science* **314**, 1439–1442.

Nakamura-Messenger K., Clemett S. J., Messenger S. and Keller L. P. (2011) Experimental aqueous alteration of cometary dust. *Meteor. Planet. Sci.* **46**, 843–856.

Nawa E., Nishigaki Y., Yamamoto D. and Shioi A. (2013) Rhythmic shape change of a vesicle under a pH gradient. *Soft Matter* **9**, 7832–7842.

Noguchi T., Ohashi N., Tsujimoto S., Mitsunari T., Bradley J. P., Nakamura T., Toh S., Stephan T., Iwata N. and Imae N. (2015) Cometary dust in Antarctic ice and snow: Past and present chondritic porous micrometeorites preserved on the Earth's surface. *Earth Planet. Sci. Lett.* **410**, 1–11.

Noguchi T., Yabuta H., Itoh S., Sakamoto N., Mitsunari T., Okubo A., Okazaki R., Nakamura T., Tachibana S., Terada K., Ebihara M., Imae N., Kimura M. and Nagahara H. (2017) Variation of mineralogy and organic material during the early stages of aqueous activity recorded in Antarctic micrometeorites. *Geochim. Cosmochim. Acta* **208**, 119–144.

Nuevo M., Milam S. N., Sandford S. A., De Gregorio B. T., Cody G. D. and Kilcoyne A. L. D. (2011) XANES analysis of organic residues produced from the UV irradiation of astrophysical ice analogs. *Adv. Space Res.* **48**, 1126–1135.

Peeters Z., Changela H. G., Stroud R. M., Alexander C. M. O'D. and Nittler L. R. (2012) Coordinated analysis of in situ organic material in the CR chondrite QUE 99177. *Lunar Planet. Sci.* **XLIII**, #2612.

Pizzarello S., Williams L. B., Lehman J., Holland G. P. and Yarger J. L. (2011) Abundant ammonia in primitive asteroids and the case for a possible exobiology. *Proc. Nat. Acad. Sci. USA* **108**, 4303–4306.

Qu H., Harada M. and Okada T. (2015) Ion-transfer voltammetry at the interface between organic and salt-doped ice phases. *ChemElectroChem* **2**, 1249–1253.

Rotundi A., Baratta G. A., Borg J., Brucato J. R., Busemann H., Colangeli L., d'Hendecourt L., Djouadi Z., Ferrini G., Franchi I. A., Fries M., Grossemy F., Keller L. P., Mennella V., Nakamura K., Nittler L. R., Palumbo M. E., Sandford S. A., Steele A. and Wopenka B. (2008) Combined micro-Raman, micro-infrared, and field emission scanning electron microscope analyses of comet 81P/Wild 2 particles collected by Stardust. *Meteorit. Planet. Sci.* **43**, 367–397.

Russell M. J., Daniel R. M., Hall A. J. and Sherringham J. A. (1994) A hydrothermally precipitated catalytic iron sulphide membrane as a first step toward life. *J. Mol. Evol.* **39**, 231–243.

Sakamoto K., Nakamura T., Noguchi T. and Tsuchiyama A. (2010) A new variant of saponite-rich micrometeorites recovered from recent Antarctic snowfall. *Meteorit. Planet. Sci.* **45**, 220–237.

Schmitt-Kopplin P., Gabelica Z., Gougeon R. D., Fekete A., Kanawati B., Harir M., Gebefuegi I., Eckel G. and Hertkorn N. (2010) High molecular diversity of extraterrestrial organic matter in Murchison meteorite revealed 40 years after its fall. *Proc. Natl. Acad. Sci. USA* **107**, 2763–2768.

Schouten S., de Graaf W., Sinninghe Damsté J. S., van Driel G. B. and de Leeuw J. W. (1994) Laboratory simulation of natural sulphurization: II. Reaction of multi-functionalized lipids with inorganic polysulphides at low temperatures. *Org. Geochem.* **22**, 825–834.

Shiraishi K. (2012) Dome fuji station in east Antarctica and the Japanese antarctic research expedition. *Proc. Int. Astron. Union* **8**, 161–168.

Stewart S. T. and Ahrens T. J. (2004) A new H_2O ice Hugoniot: implications for planetary impact events. *AIP Conf. Proc.* **706**, 1478–1483.

Taylor L. A., Nazarov M. A., Shearer C. K., McSween H. Y., Cahill J., Neal C. R., Ivanova M. A., Barsukova L. D., Lentz R. C., Clayton R. N. and Mayeda T. K. (2002) Martian meteorite Dhofar 019: a new shergottite. *Meteor. Planet. Sci.* **37**, 1107–1128.

Thomas K., Keller L.P., Blanford G. E. and McKay D. S. (1994) Quantitative analyses of carbon in anhydrous and hydrated interplanetary dust particles. In M. E. Zolensky, T. L. Wilson, F. J. M. Rietmeijer, G. J. Flynn (Eds.), Analysis of interplanetary dust, pp. 165–172.

Toppani A., Libourel G., Engrand C. and Maurette M. (2001) Experimental simulation of atmospheric entry of micrometeorites. *Meteor. Planet. Sci.* **36**, 1377–1396.

van Dongen B. E., Schouten S., Baas M., Geenevasen J. A. J. and Sinninghe Damsté J. S. (2003) An experimental study of the low-temperature sulfurization of carbohydrates. *Org. Geochem.* **34**, 1129–1144.

Vollmer C., Brenker F. E., Hoppe P. and Stroud R. M. (2009a) Direct laboratory analysis of silicate stardust from rRed giant stars. *Astrophys. J.* **700**, 774–780.

Vollmer C., Hoppe P., Stadermann F. J., Floss C. and Brenker F. E. (2009b) NanoSIMS analysis and Auger electron spectroscopy of silicate and oxide stardust from the carbonaceous chondrite Acfer 094. *Geochim. Cosmochim. Acta* **73**, 7127–7149.

Watanabe H., Otsuka T., Harada M. and Okada T. (2014) Imbalance between anion and cation distribution at ice interface with liquid phase in frozen electrolyte as evaluated by fluorometric measurements of pH. *J. Phys. Chem. C.* **118**, 15723–15731.

Yada T., Floss C., Stadermann F. J., Zinner E., Nakamura T., Noguchi T. and Lea S. (2008) Stardust in Antarctic micrometeorites. *Meteorit. Planet. Sci.* **43**, 1287–1298.

Yurimoto H., Nagashima K. and Kunihiro T. (2003) High precision isotope micro-imaging of materials. *Appl. Surf. Sci.* **203–204**, 793–797.

Zolensky M. E., Barrett B. and Browning L. (1993) Mineralogy and composition of matrix and chondrule rims in carbonaceous chondrites. *Geochim. Cosmochim. Acta* **57**, 3123–3148.

Zolensky M. E. and Barrett R. A. (1994) Composition variations of olivines and pyroxenes in chondritic interplanetary dust particles. *Meteoritics* **29**, 616–620.

Zolensky M. et al. (2006) Mineralogy and petrology of comet Wild 2 nucleus samples. *Science* **314**, 1735–1739.

Associate editor: Eric Quirico